

## IPHAS A-type Stars with Mid-IR Excesses in Spitzer Surveys

Antonio S. Hales<sup>1,2</sup>, Michael J. Barlow<sup>2</sup>, Janet E. Drew<sup>3,4</sup>, Yvonne C. Unruh<sup>4</sup>, Robert Greimel<sup>5</sup>, Michael J. Irwin<sup>6</sup> and Eduardo González-Solares<sup>6</sup>

ahales@nrao.edu

### ABSTRACT

We have identified 17 A-type stars in the Galactic Plane that have mid-IR excesses at 8  $\mu\text{m}$ . From observed colors in the  $(r' - \text{H}\alpha) - (r' - i')$  plane, we first identified 23050 early A-type main sequence (MS) star candidates in the Isaac Newton Photometric H-Alpha Survey (IPHAS) point source database that are located in *Spitzer* GLIMPSE Galactic Plane fields. Imposing the requirement that they be detected in all seven 2MASS and IRAC bands led to a sample of 2692 candidate A-type stars with fully sampled 0.6 to 8  $\mu\text{m}$  SEDs. Optical classification spectra of 18 of the IPHAS candidate A-type MS stars showed that all but one could be well fitted using main sequence A-type templates, with the other being an A-type supergiant. Out of the 2692 A-type candidates 17 (0.6%) were found to have 8- $\mu\text{m}$  excesses above the expected photospheric values. Taking into account non-A-Type contamination estimates, the 8- $\mu\text{m}$  excess fraction is adjusted to  $\sim 0.7\%$ . The distances to these sources range from 0.7 – 2.5 kpc. Only 10 out of the 17 excess stars had been covered by *Spitzer* MIPS GAL survey

---

<sup>1</sup>National Radio Astronomy Observatory, 520 Edgemont Road, Charlottesville, Virginia, 22903-2475, United States; ahales@nrao.edu

<sup>2</sup>Department of Physics and Astronomy, University College London, Gower Street, London, WC1E 6BT, United Kingdom; mjb@star.ucl.ac.uk

<sup>3</sup>Centre for Astrophysics Research, University of Hertfordshire, Hatfield, Hertfordshire AL10 9AB, United Kingdom; j.drew@herts.ac.uk

<sup>4</sup>Imperial College of Science, Technology and Medicine, Blackett Laboratory, Exhibition Road, London, SW7 2AZ, United Kingdom; y.unruh@imperial.ac.uk

<sup>5</sup>Isaac Newton Group of Telescopes, Apartado de Correos 321, E-38700, Santa Cruz de la Palma, Tenerife, Spain

<sup>6</sup>Institute of Astronomy, Madingley Road, Cambridge, CB3 0HA, United Kingdom

fields, of which 5 had detectable excesses at  $24\ \mu\text{m}$ . For sources with excesses detected in at least two mid-IR wavelength bands, blackbody fits to the excess SEDs yielded temperatures ranging from 270 to 650 K, and bolometric luminosity ratios  $L_{\text{IR}}/L_{\star}$  from  $2.2 \times 10^{-3} - 1.9 \times 10^{-2}$ , with a mean value of  $7.9 \times 10^{-3}$  (these bolometric luminosities are lower limits as cold dust is not detectable by this survey). Both the presence of mid-IR excesses and the derived bolometric luminosity ratios are consistent with many of these systems being in the planet-building transition phase between the early protoplanetary disk phase and the later debris disk phase.

*Subject headings:* circumstellar matter – planetary systems: protoplanetary disks

## 1. Introduction

Multi-wavelength photometry remains the fundamental tool for detecting circumstellar (CS) dust around pre-main sequence and main sequence (MS) stars. Almost all MS stars known to be surrounded by dust disks have been discovered from the shapes of their spectral energy distributions (SEDs), which show excesses with respect to the stellar photospheres at infrared (IR) and longer wavelengths (Aumann et al. 1984). Since their discovery, great interest has arisen in these MS debris disk systems as they are thought to be signposts of planet formation (Zuckerman 2001). While resolved imaging is crucial for studying the characteristics of individual systems, photometric surveys remain the key tool for inferring their statistical evolutionary properties (Meyer et al. 2007). Many surveys for dusty MS stars have used the *Infrared Astronomical Satellite (IRAS)* database (Aumann 1985; Walker & Wolstencroft 1988; Cheng et al. 1992; Oudmaijer et al. 1992; Mannings & Barlow 1998; Sylvester & Mannings 2000; Silverstone 2000; Rhee et al. 2007). Cross-correlation with spectral catalogs allows a search for excess fluxes when compared to the expected photospheric emission.

The systems can be characterized by the amount of light absorbed and re-emitted by the disk (the disk-to-star bolometric luminosity ratio  $L_{\text{IR}}/L_{\star}$ ). Large values of  $L_{\text{IR}}/L_{\star}$  ( $> 10^{-2}$ ) are associated with massive ( $M > 0.02 M_{\odot}$ ) orbiting CS disks, typically found around young pre-MS systems ( $t \sim 10^6$  Myr), such as T Tauri and HAeBe stars. These, in addition, often show spectroscopic signatures of material still falling onto the central star (Waters & Waelkens 1998). On the other hand, low  $L_{\text{IR}}/L_{\star} < 10^{-3}$  values correspond to MS stars surrounded by older, more tenuous dusty disks (usually gas-depleted), likely to be sustained by collisions between larger bodies (debris-disks).

CS disks can also be characterized by the wavelength at which the excess first appears. Excesses detected over a broad wavelength range (from near-infrared to millimeter wavelengths) are indicative of CS disks having dust belts located at a range of orbital radii (e.g., Dullemond et al. 2007). Short wavelength excesses ( $\lambda < 3 \mu\text{m}$ ) indicate the presence of hot dust located in the innermost regions of the disk ( $r < 1 \text{ AU}$ ). Conversely, the lack of short wavelength excess flux can be modeled as due to disks with cleared inner regions, that could be caused by the presence of shepherding planets (e.g., Calvet et al. 2002; D’Alessio et al. 2005). Among disks with cleared inner region two categories are distinguishable: young gas-rich systems transitioning between their pre-MS and MS stages (e.g. 49 Cet; Hughes et al. 2008), and older debris systems that lack gas as well as planetesimal belts in the innermost regions of the disk.

The *IRAS* samples showed that the number of objects with 12- $\mu\text{m}$  excesses (but no near-IR excesses, e.g.  $\beta$  Pictoris) was significantly lower than those with excesses at longer wavelengths, 0.5 – 2% versus 10 – 20% for excesses at  $\lambda \geq 25 \mu\text{m}$  (Aumann & Probst 1991; Cheng et al. 1992; Plets & Vynckier 1999; Fajardo-Acosta et al. 2000; Lagrange et al. 2000; Song et al. 2001). The ubiquity of cold disks is consistent with evolutionary scenarios in which disk clearing occurs in an in-out way; material occupying the inner region of a protoplanetary disk, and its observational signatures, disappears before material in the outer disk (Backman & Paresce 1993; Wuchterl et al. 2000; Meyer et al. 2007; Cieza et al. 2007).

With notably improved sensitivity compared to its predecessors, *Spitzer Space Telescope* observations have confirmed that not only do the occurrence and magnitude of infrared excesses decay with time, but that in the case of MS systems, *cool* dust excesses ( $\lambda > 24 \mu\text{m}$ ,  $T < 100 \text{ K}$ ) are systematically more frequent than *hot* or *warm* ones (detected between 2-24  $\mu\text{m}$ ). The results of Beichman et al. (2005), Bryden et al. (2006) and Su et al. (2006) clearly indicate that 70- $\mu\text{m}$  excesses are more common than 24- $\mu\text{m}$  excesses for MS stars of a given age, but the different incidence fractions quoted appear to be dominated by the varying volumes and targeted spectral types of each sample (FGK stars in the first two cases, and A-type stars in the work of Su et al. 2006). Systems with excesses at mid-IR wavelengths (but without near-IR excesses or other signs of ongoing accretion) are far less common (Silverstone et al. 2006; Sicilia-Aguilar et al. 2006; Meyer et al. 2007; Uzpen et al. 2007). Silverstone et al. (2006) carried out 3.6–8  $\mu\text{m}$  observations of 74 young ( $t < 30 \text{ Myr}$ ), Sun-like stars ( $0.7 M_{\odot} < M < 1.5 M_{\odot}$ ), in order to investigate the presence of hot (220–1000 K) dust in the inner regions of CS disks and found evidence for only 5 optically thick disks, which were more likely to be pre-MS T Tauri stars and not transition- or  $\beta$  Pictoris-like systems. Uzpen et al. (2007) cross-correlated the *MSX* (Egan et al. 1997) and *Spitzer* GLIMPSE (Churchwell et al. 2005) catalogs with the Tycho 2 Spectral Catalog (Wright et al. 2003) and inferred the incidence of 8- $\mu\text{m}$  excesses to be as low as 1 – 2 % for Galactic MS

systems of spectral type B8 or later. A large fraction of the GLIMPSE catalog is still unexplored, as most cataloged sources lack spectral classifications.

In this work we exploit several Galactic Plane surveys in order to search a very large sample of A-type MS stars for 8- $\mu\text{m}$  excesses. One of the main aims of this work was to investigate the incidence of mid-IR excesses around a large unbiased sample of early A-type stars. This sample covers previously unexplored magnitude and distance ranges, allowing us to detect the optical, near-IR and mid-IR photospheric emission from A-type dwarfs out to distances of  $\sim 2.5$  kpc. Being abundant, luminous and devoid of circumstellar free-free emission (which can lead to false excesses as in the case of B-stars, e.g. Clarke et al. 2005), A-type dwarfs are excellent targets to search for CS dust emission. A large fraction (50%) of the debris-disks systems known to date orbit A-type dwarf stars (Silverstone 2000; Rhee et al. 2007). Our MS A-type sample, drawn from the INT/WFS Photometric H-alpha Survey of the Northern Galactic plane (IPHAS, Drew et al. 2005; Gonzalez-Solares et al. 2008), is selected from their observed optical ( $r' - i'$ ) and ( $r' - H_\alpha$ ) IPHAS colors. This color selection scheme ensures most selected objects are near or on the MS, excluding pre-MS (such as Herbig Ae stars) and post-MS objects with prominent  $H_\alpha$  emission. Cross-correlating with near- and mid-IR sources from the 2MASS and GLIMPSE surveys enables their dereddened 0.6  $\mu\text{m}$  to 8  $\mu\text{m}$  SEDs to be constructed, in order to search for warm ( $T \sim 150 - 800$  K) mid-IR excesses. In addition, early-release post basic-calibration 24- $\mu\text{m}$  images from the *Spitzer* MIPS GAL survey (Carey et al. 2005) were used to search for 24- $\mu\text{m}$  confirmation of the mid-IR excesses.

Section 2 describes our method of selecting A-type MS stars from the IPHAS database and their cross-correlation with the *Spitzer* data. In Section 3 we identify those sources with detectable mid-IR excesses and fit black-bodies to their excesses. The properties of the sample are discussed in Section 4, with Section 5 summarising our conclusions.

## 2. Observations and data processing

### 2.1. IPHAS

#### 2.1.1. IPHAS Data

The INT/WFS Photometric H-alpha Survey of the Northern Galactic plane (IPHAS; Drew et al. 2005; Gonzalez-Solares et al. 2008) is a multi-national observing programme dedicated to surveying the northern galactic plane. The northern galactic latitude range of  $-5^\circ < b < +5^\circ$  represents a total sky area of 1800 square degrees.

Two broad-band Sloan  $r'$  and Sloan  $i'$  filters, in conjunction with a narrow band  $H\alpha$  filter, provide sufficient photometric information to identify approximate spectral types for most stars detected by the survey (Drew et al. 2008; Sale et al. 2008). The limiting magnitude of the IPHAS survey is  $r' \sim 20.5$ . By the end of data-taking in 2008-9, over 200 million objects are expected to be cataloged in terms of their positions and  $r'$ ,  $i'$  and  $H\alpha$  magnitudes.

IPHAS observations are made using the Wide Field Camera (WFC) at the 2.5-m Isaac Newton Telescope (INT), La Palma, Spain. The WFC, an imager made of four  $4k \times 2k$  EEV CCDs arranged in an L shape, provides a field of view of  $34 \times 34$  arcmins. The pixel size of 0.3333 arcsec is sufficient to provide high quality sampling of the  $\sim 1$  arcsecond seeing encountered at the Observatorio del Roque de los Muchachos. The  $r'$  filter has a central wavelength of 6240 Å. The  $H\alpha$  filter has a FWHM transmission of 95 Å, centered at 6568 Å, towards the red end of the  $r'$  filter. The  $i'$  filter has a central wavelength of 7743 Å. In order to account for the gaps between CCDs on the WFC, observations for a given field of view are paired with a second observation offset 5 arcmin-West and 5 arcmin-South. These are usually referred to as the *on* and *off* exposures of a given field. The total number of pointings required to cover the survey area is 7635, with most sources being imaged at least twice. The exposure time in the  $H\alpha$  filter was 120s, while for the  $r'$  filter the exposure time was 30s and for the  $i'$  filter it was 10s. The saturation limits ( $r' \sim 13.5$  mag) are discussed by Drew et al. (2005) and Gonzalez-Solares et al. (2008).

The data are processed at the Cambridge Astronomical Survey Unit (CASU<sup>1</sup>) as described by Irwin (1985) and Gonzalez-Solares et al. (2008). Sources are classified following their extraction characteristics, e.g.,  $0 = \text{noise like}$ ,  $1 = \text{non-stellar}$ ,  $-1 = \text{stellar}$ ,  $-2 = \text{probably stellar}$ ,  $-9 = \text{saturated}$ . Photometric standards observed during the night are used for flux calibration in each passband. Astrometric solutions are initially derived based on the known telescope and camera characteristics, and then refined using the 2MASS catalogue (Gonzalez-Solares et al. 2008). The distribution of position discrepancies between IPHAS and 2MASS is roughly Gaussian, with a peak at 0.0 arcsec, and has a standard deviation of 0.1 arcsec. Hence, the astrometric precision of IPHAS with respect to 2MASS is assumed to be better than 0.1 arcsec (Gonzalez-Solares et al. 2008).

In recent processing (Gonzalez-Solares et al. 2008), the nightly  $H\alpha$  zeropoint is set at a constant offset of 3.14 with respect to the  $r'$  zeropoint, defined by the flux difference between the narrowband and  $r'$  transmission profiles convolved with Vega's spectrum (Bohlin 2007).

---

<sup>1</sup><http://apm2.ast.cam.ac.uk/cgi-bin/wfs/dqc.cgi>

This assures that  $(r' - H\alpha)$  is brought to zero for unreddened Vega-like stars. At the time the work was carried out for this paper an earlier method of  $H\alpha$  calibration was in use that meant the  $(r' - H\alpha)$  was not anchored in this way (see, Drew et al. 2005). This had implications for the extraction of A-dwarf candidates which we discuss below. After processing, a final catalog for a single pointing can contain from ten to fifty thousand objects (stellar and non-stellar).

### 2.1.2. A-dwarfs in the $(r' - i')$ versus $(r' - H\alpha)$ plane

The equivalent width of the photospheric  $H\alpha$  absorption feature peaks at early A-types. As a consequence, for a given  $r'$  magnitude and reddening, the  $(r' - H\alpha)$  color of an A-type star will be a minimum compared to that of other stellar types. Drew et al. (2005) computed the synthetic IPHAS  $(r' - H\alpha)$  and  $(r' - i')$  colors for stars of various luminosity classes and spectral types present in the catalog of stellar SEDs by Pickles (1998), and investigated their variations for different amounts of interstellar reddening. Figure 1 (left-panel, adapted from Drew et al. (2005)), shows a synthetic IPHAS color-color diagram. The positions of main sequence, giant and supergiant stars are mapped for three different values of  $E(B - V)$ . It can be seen that, as the reddening increases, the minima of the loci of MS stars trace out an approximately parabolic line. Due to their strong  $H\alpha$  absorption, this line traces the positions of MS early A-type stars in the  $(r' - i')$ ,  $(r' - H\alpha)$  plane as a function of reddening. Consequently it has been named the *early-A reddening line*. Objects near this line will mostly be A0-5 near-MS stars. How this is so and how these stars may be extracted and exploited has been presented Drew et al. (2008).

### 2.1.3. Selection of A-dwarf stars

In order to obtain a sample of early A-type stars that can be cross-correlated with the GLIMPSE point-source catalog, all the available IPHAS data for regions that overlapped with the GLIMPSE survey were downloaded ( $30^\circ < l < 65^\circ$  and  $|b| < 1^\circ$ ). To ensure the quality of the sample, we restricted the search to objects having  $r'$  magnitudes between  $14 < m_{r'} < 18$  and to fields that had seeing better than 2 arcsec. In addition, objects had to be flagged as stellar or probably stellar by CASU in all 6 IPHAS exposures to be selected ( $r'$ ,  $i'$  and  $H\alpha$  in both on- and off- observations). Only 44% (134 of 298) of the IPHAS fields for this region had been obtained at the time that this investigation commenced. A complete list of the relevant processed IPHAS catalogs is presented in Table 1. The central coordinates

of each pointing are listed in both Equatorial J2000 and Galactic coordinates, arranged in order of increasing galactic longitude. Column 6 gives the average seeing measured at the Observatorio del Roque de los Muchachos during the *on* and *off* integrations for each field. Field numbers (column 1) correspond to internal IPHAS field names.

In each IPHAS field, the lower edge of the main stellar locus in the  $(r' - i', r' - H_\alpha)$  plane will always follow the aforementioned early-A reddening line. Therefore, this line can be used as the cut line for selecting A-type stars (Drew et al. 2008). First, the position of the early-A reddening line had to be defined interactively, allowing for an empirical  $(r' - H_\alpha)$  shift to deal with the floating  $H_\alpha$  zero-point magnitude, then in use (in principle the early-A reddening line should originate close to  $(r' - i', r' - H_\alpha) = (0,0)$ , but the variable  $H_\alpha$  zero-point magnitude requires that the origin of the A-type reddening line has to be placed interactively for each IPHAS field).

Once a good alignment between the A-type reddening line and the lower edge of the loci of MS stars has been achieved, all stars located between the fitted early-A reddening line and a second cutoff line will be selected as A-type candidates. This defines an early-A reddening  $(r' - H_\alpha)$  strip, starting from the location of the fitted early A-type reddening line upward (e.g. as in Figure 1, right-hand panel). The choice of width for each field was made after inspection of the color-color diagram for each field individually. The guiding principle was to make this width large enough to be inclusive of the great majority of A dwarfs. This approach inevitably admits some interlopers, mainly of somewhat later spectral type, but these can be eliminated at the later SED-fitting stage of the analysis. The width of the  $(r' - H_\alpha)$  strip was required to never exceed 0.07 mag and was typically 0.05 mag (cf. the detailed discussion by Drew et al. (2005) of this point). Once the early-A reddening strip had been defined, the programme identified all stars lying within the strip and extracted the corresponding stellar coordinates, together with their photometric information ( $r', i', H_\alpha$  magnitudes, associated uncertainties, extraction parameters, and 2MASS JHK photometry, if available).

Table 1, column 7, summarizes the numbers of objects cataloged in each field, which provide the input for A-type star extractions. Column 8 shows the number of A-type dwarfs extracted for each IPHAS field. Of a total of 260,223 input stars, 23,050 were selected as early A-type dwarfs on the basis of their IPHAS colors, corresponding to 8.8% of the total field stars.

## 2.2. GLIMPSE

GLIMPSE - the Galactic Legacy Infrared Mid-Plane Survey Extraordinaire (Churchwell et al. 2005) - is a fully sampled, confusion limited, 4-band near- to mid-infrared survey of the inner third of the Galactic disk, with a spatial resolution of 2 arcseconds at the shortest wavelengths (Benjamin et al. 2003). Using the Infrared Array Camera (IRAC, Fazio et al. 2004), GLIMPSE imaged 220 square degrees at wavelengths centred on 3.6, 4.5, 5.8, and 8.0  $\mu\text{m}$  in the Galactic longitude range 10 to 65 degrees on both sides of the Galactic Centre, over a Galactic latitude range of  $\pm 1$  degrees. The photometric sensitivity of 0.3 mJy achieved by GLIMPSE at 8  $\mu\text{m}$  in lower background areas (see Table 2) can allow the unreddened photospheres of early A-type dwarfs to be detected out to nearly 2 kpc, and is the deepest mid-IR survey of the Galactic plane carried out to date. GLIMPSE data products come as point-source catalogs and flux-calibrated mosaic images for each IRAC band, available at the *Spitzer* Science Centre (SSC<sup>2</sup>) server. The nominal 8  $\mu\text{m}$  flux-limit of the GLIMPSE Highly-Reliable Catalog of 10 mJy would imply that bare photospheres of A-type stars can be detected out to distances of  $\sim 600$  pc.

The GLIMPSE Highly-Reliable Catalog contains point-like sources whose selection requirements meet a 95% reliability criterion, determined by the fact that a source must be detected twice in one band and at least once in an adjacent band. This is called the *2+1* criterion. The fluxes in the two bands satisfying the *2+1* criterion must be higher than the flux limits listed in Table 2 and are required to have signal-to-noise ratios (S/N) greater than 5. For the other two bands, the fluxes may be lower than the survey flux limits, provided they have  $S/N > 3$ . Therefore, the GLIMPSE catalog can contain sources significantly fainter at 8  $\mu\text{m}$  than the nominal 10 mJy limit. For the 4 s integrations used by GLIMPSE, the estimated 8  $\mu\text{m}$   $5\sigma$  point-source sensitivity for low backgrounds is 0.4 mJy, equivalent to 13th magnitude<sup>3</sup>. The catalog contains  $\sim 31$  million sources.

The IPHAS A-type sample was correlated with the GLIMPSE catalog, imposing a maximal radial separation of 1 arcsec. No multiple associations were found at this matching radius. Column 9 in Table 1 summarizes the results from the IPHAS-GLIMPSE A-type star correlation procedure. Of the 23050 IPHAS-selected A-type stars, 15312 have reliable detections in at least 2 IRAC bands. Of these 15312 objects, 11198 have positive detections in all 2MASS near-IR bands. Source counts in the GLIMPSE catalog drop by a factor of

---

<sup>2</sup><http://ssc.spitzer.caltech.edu/>

<sup>3</sup><http://www.astro.wisc.edu/sirtf/>



three from IRAC 3.6 and 4.5  $\mu\text{m}$  to IRAC 5.8 and 8  $\mu\text{m}$  (Benjamin et al. 2005). This is reflected in the number of correlated sources detected at 5.8 and 8  $\mu\text{m}$  (5111 and 2751 stars respectively, as shown in Table 3). Imposing the requirement that the selected stars must be detected in all 2MASS and IRAC bands led to a sub-sample of 2692 A-type stars with fully sampled 0.6 to 8- $\mu\text{m}$  SEDs. These 2692 stars obtained from the IPHAS/GLIMPSE correlation will be referred as the GLIPHAS sample hereafter.

The distribution of positional discrepancies between the GLIMPSE positions versus the 2MASS positions for the GLIPHAS sample peaks at 0.23 arcsec, with typical dispersions of 0.07 arcsec (as described in both the GLIMPSE Data Release and in the GLIMPSE Quality Assurance documentation available in the Team’s website). Therefore, there is an average systematic offset of 0.2-0.3 arcsec between the GLIMPSE and 2MASS positions which should reflect in the IPHAS-GLIMPSE correlation (since the IPHAS positions are tied to 2MASS). The distribution of radial distances between the IPHAS and GLIMPSE positions is shown in Figure 2. The distribution is approximately Gaussian, peaks at 0.36 arcsec and has a standard deviation of 0.11 arcsec. The mean IPHAS-GLIMPSE offset of 0.36 arcsec is slightly larger than the 0.2-0.3 arcsec expected by assuming the IPHAS-2MASS mean offset is zero and the GLIMPSE-2MASS mean offset is 0.23 arcsec. However, as stated in the GLIMPSE Data Release documentation, the offsets between GLIMPSE and 2MASS sources can be larger for fainter sources due to poor centroiding. As we are tackling the faint end of the GLIMPSE dataset, we believe this may be responsible for the small increase between the GLIMPSE-2MASS and IPHAS-GLIMPSE mean offsets.

The probability of possible confusing sources can be estimated by considering the average source density of the two catalogues over the surveyed area, multiplied by the area of each cross-correlation ( $\pi \times 1.0^2$ ). There are  $\sim 7$  million GLIMPSE sources within the surveyed region ( $30^\circ < l < 65^\circ$  and  $|b| < 1^\circ$ ). However, most IPHAS A-type stars will have 3.6- $\mu\text{m}$  magnitudes brighter than 14 (based on reddening estimates from the  $(r' - i')$  colors and assuming A-type colors; Section 3 for details). After removing stars with  $[3.6] > 14$ , there are  $6.05 \times 10^6$  GLIMPSE stars that could possibly contaminate the IPHAS cross-correlation (corresponding to a source density of  $6.6 \times 10^{-3} \text{arcsec}^{-2}$  over the  $\sim 70 \text{deg}^2$  surveyed area). Therefore there is a 2% chance of false positives in the search for positional coincidences, implying that amongst the 2692 GLIPHAS A-type stars there could be up to 56 contaminating objects ( $6.6 \times 10^{-3} \times \pi \times 1.0^2 \times 2692 = 56$ ).

### 2.3. WHT optical spectra of IPHAS-selected A-type stars

Optical spectra of 18 IPHAS A-type star candidates, 10 of which are in the GLIPHAS sample, have been acquired in order to test the reliability of our photometric spectral-type selection method. The data were acquired using the Intermediate dispersion Spectrograph Imaging System (ISIS) on the 4.2-m William Herschel Telescope (WHT) during the nights of 2006 August 23 and 24, using two different gratings to simultaneously cover the blue (central wavelength 4249 Å) and red (7506 Å) regions. Seeing conditions ranged between 1.2 to 2 arcsec on both nights.

Standard data-reduction procedures were performed using the FIGARO Starlink<sup>4</sup> application. These included bias-subtraction, flat-fielding, sky-subtraction, extraction, wavelength calibration and relative flux calibration. The red exposures showed strong fringing (typically on scales of the order of 10 to 20 pixels). This, along with other pixel-to-pixel variations, was removed during the flat-fielding process. No attempt was made to correct for the grating efficiency using the flat-field exposures; it was instead removed during the flux calibration. The spectral resolution as measured from the FWHM of arc lines was found to be 4.25 Å in the blue and 3.32 Å in the red. The dispersion solution was estimated to be good to 0.01 Å in the red region, while in the blue it was found to be accurate to 0.04 Å. Flux calibration was performed using the optimal extraction method (Horne 1986) using BD+28°4211 (Oke 1990) as a relative flux calibrator.

Spectral classification was performed by comparing the WHT spectra with early-type template spectra from the Indo-US Library of Coudé Feed Stellar Spectra ( $\sim 1$  Å resolution, Valdes et al. 2004), after degrading the library spectra to match the spectral resolution of the data. The observed spectra were dereddened using the visual extinction estimates from the IPHAS colors (Table 7, see Section 3.1 for details), and then matched by eye to the closest spectral type using a spectral type grid ranging from B6V to F5V. The Ca II K line (3933.66 Å) is a crucial spectral type diagnostic for early-type stars, but can potentially be affected by interstellar Ca II absorption over 1-2 kpc sight-lines. The Ca II IR triplet (8498.02, 8542.09, and 8662.14 Å) does not suffer from this problem and due to the lower reddening in this spectral region the lines are observed with good S/N. We therefore carried out two different spectral type assignments for each star, one based on the blue spectrum, in which the Balmer lines and Ca II K-line of target and template stars were compared, and one based on the red spectrum, where the Paschen and Ca II IR-triplet lines of target and templates were compared. The comparison between the template spectrum and the 10 GLIPHAS spectra is shown in Figure 3. With the exception of WHT 4 (see below), all

---

<sup>4</sup><http://www.starlink.rl.ac.uk/>

18 stars that were observed were classified as near main sequence A-type. The blue- and red-based spectral type assignments for the 10 GLIPHAS stars are presented in Table 4, together with the measured equivalent widths of the Ca II K-line and the IR-triplet lines. The red-based spectral types range from A0V to A5V, and are systematically earlier than the blue subtypes, by at least a sub-type. This is as would be expected if the blue-based classifications suffer from interstellar Ca II-K contamination, leading to an apparently later spectral type. In section 3 the dereddened SEDs of all stars with WHT spectra are shown against a reference A3V stellar SED. In all cases the SED of the observed star is confirmed to follow the SED of an A-type star. The optical spectra and the overall SEDs both demonstrate the reliability of our method of selecting A-type stars based on their IPHAS colors.

No blue flux was detected from WHT 4, so no blue-based spectral classification was possible. In addition, its IR-triplet lines were too deep to be fitted by any A-dwarf spectra. This could be explained by WHT 4 being a giant or a supergiant, since a lower surface gravity leads to deeper and narrower lines. A higher luminosity star would be consistent with the lack of blue flux, since it would be located much further away and more highly reddened. Comparison of its spectrum with those of the giant and supergiant templates from the Indo-US library showed that it could be well matched to the spectrum of an A5 supergiant (A5Ia). For an  $M_v$  of  $-7.4$  (Schmidt-Kaler 1982) this would correspond to a spectrophotometric distance of 4.6 kpc, close to the location of the Scutum-Crux Arm (Bronfman 1992; Russeil 2003) and much more in keeping with its large reddening ( $A_{r'} = 9.3$ ) than the distance of 100 pc that would be derived assuming the object is a dwarf (see Table 5).

## 2.4. MIPS GAL

MIPSGAL (Carey et al. 2005) is a *Spitzer* legacy survey that covers 220 square degrees of the inner Galactic plane ( $65^\circ < l < 10^\circ$  and  $-10^\circ < b < -65^\circ$  for  $|b| < 1^\circ$ ) at 24 and 70  $\mu\text{m}$  with the Multiband Imaging Photometer for *Spitzer* (MIPS, Rieke et al. 2004). It has significantly better resolution and sensitivity than previous infrared surveys covering the plane at these wavelengths. MIPSGAL complements the Galactic Disk area covered by GLIMPSE. The MIPSGAL survey was not complete at the time this investigation was begun, with only post basic-calibration (PBCD) mosaic images of a few sky regions being available.

In Section 3, we searched for GLIPHAS stars with excess 8  $\mu\text{m}$  fluxes with respect to the expected photospheric emission. For the 17 GLIPHAS stars found to have 8  $\mu\text{m}$  excesses (presented in Section 3.1), we inspected mosaic images from the MIPSGAL survey in order

to search for possible 24- $\mu\text{m}$  detections. The availability of 24- $\mu\text{m}$  data-points can be used as confirmation of a mid-IR excess and to provide better constraints when modelling the properties of the emitting dust.

Since only the 24- $\mu\text{m}$  PBCD images could be used for science analysis<sup>5</sup>, only the 24- $\mu\text{m}$  images were downloaded. The images are calibrated in units of MJy/sr and so can be used for flux estimation purposes. The zeropoint used by us to convert 24- $\mu\text{m}$  fluxes to magnitudes was 7.14 Jy, as computed from an extrapolation of a model spectrum of Vega (provided by the SSC). Based on preliminary analysis of mosaic images for low-background regions, sources with fluxes down to 1 mJy could be extracted. This corresponds to a 24  $\mu\text{m}$  magnitude of approximately 9.6.

The MIPS images were visually inspected at the positions of each of the 17 GLIPHAS stars with 8  $\mu\text{m}$  excesses (presented in Section 3.1, Tables 6 and 7). 5 of the 17 stars had point-like counterparts located within 1 pixel (2.45 arcseconds) of the registered IPHAS position, and were selected for flux extraction. Upper-limits for 5 other stars were also derived, while the positions of the remaining 7 stars had not been covered by the currently available MIPS GAL images.  $5\sigma$  24- $\mu\text{m}$  upper limits for the 5 non-detected sources were computed using the formula given by Uzpen et al. (2007), assuming a diffraction-limited aperture size and a rms flux limit computed within a  $25 \times 25$  pixel box centered at the position of the star.

The 24  $\mu\text{m}$  fluxes of the detected stars were measured in the following way: an average Point Response Function (PRF) was constructed for each image by selecting a few stars of similar brightness to the candidate star. PRF reference stars located close to the candidate were preferred in order to avoid known PRF variations across the mosaic images. The Image Reduction and Analysis Facility (IRAF<sup>6</sup>) package DAOPHOT was used to create the PRF and to extract the candidate object flux.

Once created, this PRF was used to fit the image of the candidate star and to extract its flux, using an aperture of 5 pixels (12.45 arcseconds). The sky background was defined as the mode value within an annular region of 4 pixels in width and located 9 pixels in radius away from star. This background estimation was subtracted when calculating the star's flux. Photometric uncertainties are the statistical errors. Residual images were produced and in-

---

<sup>5</sup>see the MIPS data-handbook, at <http://ssc.spitzer.caltech.edu/mips/dh/>

<sup>6</sup><http://iraf.noao.edu/>

spected for possible extraction artifacts or over/under-subtraction. An aperture correction of 1.17 was applied to the derived fluxes, taken from the MIPS Data Handbook.

For all 5 detected sources the fitted positions agreed to within less than 0.5 arcseconds with the cataloged IPHAS sky coordinates, suggesting that they are indeed associated with the A-type stars from our IPHAS-GLIMPSE sample. The 24- $\mu\text{m}$  fluxes and upper limits are presented and discussed in Section 3.

### 3. A-type Stars with Mid-infrared Excesses

#### 3.1. IPHAS-GLIMPSE A-stars with 8- $\mu\text{m}$ excesses

We searched for stars with 8- $\mu\text{m}$  excesses amongst the 2692 A-type stars from the GLIPHAS sample, initially by looking for unusually large ( $K-8$ ) colors (e.g., Aumann & Probst 1991; Uzpen et al. 2005, 2007). Since the stars of our sample should be mostly early A-type stars, their dereddened colors correspond closely to their color excesses. Our IPHAS color-color selection criterion is expected to extract stars with spectral types mainly in the range A0V to A5V. Consistent with the discussion presented by Drew et al. (2008), we adopt  $M_{r'} = 1.55$ , and intrinsic  $(r' - i') = 0.05$  as representative of the target early-A dwarfs (cf. Houk et al. (1997) Hipparcos absolute magnitudes, and Kenyon & Hartmann (1995) colors).

The observed magnitudes were dereddened using the optical and near-IR reddening laws of Schlegel et al. (1998) (after converting the 2MASS magnitudes to UKIRT  $JHK$  magnitudes using the solutions from Carpenter (2001), as the Schlegel et al. (1998) extinction coefficients are in the UKIRT system). For the IRAC bands, the extinction coefficients derived by Indebetouw et al. (2005) were used.

As outlined by Drew et al. (2008), the color excess due to extinction,  $E(B-V)$ , can be derived by subtracting the intrinsic color (0.05) from the observed  $(r' - i')$  color to give  $E(r' - i')$ , which is then multiplied by 1.55. To obtain the visual extinction,  $A_v$ ,  $E(r' - i')$  should be multiplied by 4.901 (Schlegel et al. 1998).

However, given the long sightlines addressed in this work, it makes more sense to refer all reddenings to either the  $r'$  or the  $i'$  band, rather than to  $V$  in view of the fact that atypical laws vary away from the norm most strongly in the blue-to-visual part of the optical spectrum (Cardelli et al. 1989). Specifically, the following relations were applied:  $A_{r'} = 4.13 \cdot E(r' - i')$ , and  $A_{i'} = 3.13 \cdot E(r' - i')$  (using tabulated data from Schlegel et al. 1998).

Color excesses were calculated by taking the differences between the dereddened magnitudes, since the intrinsic colors are expected to be close to 0.0 for early A-type stars. Figure 4 shows the dereddened  $(J - H, K - 8)$  color-color diagram for the 2692 stars with measured fluxes in all IPHAS, 2MASS and IRAC bands. The dereddened  $(J - H)$  colors of the sample cluster around a mean of 0.03, consistent with most of them being A stars (recalling that mean  $(J - H)$  for unreddened A0-5 stars ranges from 0.0 to 0.06; Kenyon & Hartmann 1995). The standard deviation, 0.12 mags, will be mainly due to photometric errors, which are amplified in the dereddening process, and perhaps partially due to contamination of the sample by stars that are not A type. Indeed there is a modest redward skew of the dereddened  $(J - H)$  distribution that could be induced by contaminant objects, being more commonly of later spectral type than A0-5, than earlier: specifically 36 stars (1.3 % of the total sample) are present with  $(J - H) > 0.36$ ,  $3\sigma$  more red than the mean, while only 1 star (0.04 %) lies in the blue tail with  $(J - H) < 0.04$ . Furthermore, whilst it is likely that the majority of the sample are near the main sequence, it is important to bear in mind also that this color selection on its own does not exclude more luminous evolved objects. We can place a figure on the likely level of contamination after examining the excess  $(K - 8)$  objects.

$E(K - 8)$  color excesses were calculated by taking the differences between the dereddened  $K$  and  $8\text{-}\mu\text{m}$  magnitudes, since the intrinsic  $(K - 8)$  color is expected to be close to 0.0 for A0-5 stars. The distribution of  $E(K - 8)$  is not Gaussian, as shown in Figure 5, right-hand panel (the Shapiro-Wilk test for normality was performed and the null hypothesis of normality was rejected at 99% confidence level). It has a mean of 0.05, a standard deviation of 0.29, and a median of 0.00. 34 objects with  $E(K - 8)$  larger than 3 times the standard deviation from the mean (i.e.  $E(K - 8) > 0.9$ ) were removed and statistics recomputed for the main sample. This procedure was repeated until the statistics converged to a mean  $E(K - 8) = 0.03$  and standard deviation of 0.22. The Shapiro-Wilk test was recomputed but again argued against normality of the sigma-clipped sample. The width of the  $E(K - 8)$  distribution for the sigma-clipped sample cannot be attributed purely to photometric errors, as the distribution of  $(K - 8)$  errors peaks at the mean value  $\sigma_{phot}^2 = 0.15$  and has a dispersion of 0.07. From this comparison one can estimate the additional source of errors introduced to the color excesses from the dereddening procedure. Assuming  $\sigma_{K-[8]}^2 = \sigma_{phot}^2 + \sigma_{dered}^2$ , the above numbers imply  $\sigma_{dered} = 0.16$ .

Given that the distribution is not Normal (not even after convergence of the iterative sigma-clipping of a total of 58 outliers with  $E(K - 8)$  larger than 3 times the standard deviation from the mean), we searched for  $E(K - 8)$  excess objects by comparing the difference between the observed color for every source and the mean of the sigma-clipped sample, divided by the quadratic sum of each’s star photometric uncertainty and the standard deviation of the clipped sample. In this manner, we define the signal-to-noise (SN) ratio of

an  $E(K - 8)$  excess as  $SN = \frac{E(K-8)-0.03}{(\sigma_{K-8}^2+0.22^2)}$ . The distribution of SN for the entire sample of 2692 stars is shown in the left-hand panel of Figure 5. The distribution is approximately Gaussian, peaks at 0.0, and has a positive tail due to the presence of possible  $E(K - 8)$  excess sources. There are no sources with  $SN < -3$  and conversely, we adopt  $SN > 3$  as the threshold for considering an  $E(K - 8)$  excess to be present. A total of 20 stars are found to have  $SN > 3$ , and are highlighted by diamond symbols in the color-color diagram in Figure 4.

Assuming that the K-band flux is photospheric and that the color excess is due purely to an 8 micron flux excess, one could conclude these 20 stars with 8- $\mu\text{m}$  excesses correspond to a real population of objects with continuum excesses. The SEDs of the twenty 8- $\mu\text{m}$  excess stars have been constructed and inspected to check whether they conform to those of A0-5 stars. In this step we found that three had SEDs deviating significantly from this expectation, in that they more strongly resembled cooler spectral types. Since the  $E(K - 8)$  selection should not bias in favour of an A spectral type, this failure rate provides us with a rough estimate of the non-A-type contamination of the IPHAS-selected sample as a whole: 3 interlopers out of 20 implies  $15 \pm 4\%$  of the full sample may not be A stars. All three stars are excluded from further analysis. Follow-up spectroscopy of a subsample of 4 of the 17 excess stars that passed the SED test confirms that all give a good match to main sequence A-dwarf template spectra (J191100+094543, J192914+184004, J192933+183415 and J194541+243253, as listed in Table 4). Comparison of the SEDs of the other 14 IPHAS candidate A-stars having follow-up WHT spectra (and that do not have an 8- $\mu\text{m}$  excess) also indicate they match well an A3V SED, as shown in Figure 6 for the six that are in the GLIPHAS sample.

Table 5 lists the optical to mid-IR photometry for the 6 GLIPHAS stars with no distinguishable IR-excess for which WHT spectra were obtained, while Table 6 lists the photometry for the 17 GLIPHAS A-type stars selected as having 8- $\mu\text{m}$  excesses. In the 5 cases where a 24- $\mu\text{m}$  flux was detected and extracted according to the procedure described in Section 2.4, the recovered 24 $\mu\text{m}$  magnitudes are also listed. The 24- $\mu\text{m}$  fluxes were not dereddened, as extinction is expected to be negligible at this wavelength.

### 3.2. Modeling the mid-IR excesses

In order to characterise the strength of the mid-IR excesses, we employed a solar-metallicity Kurucz model atmosphere (Kurucz 1979) with  $T_{eff} = 9000$  K,  $\log g = 4.0$  to extrapolate the observed  $K$ -band flux to longer wavelengths. On normalising the model SED flux to the observed fluxes in the  $K$  band, we obtain a good fit to the optical and near-IR datapoints, confirming the reliability of the IPHAS A-type selection method. The

mid-IR excesses (excess above photosphere, in mJy) were calculated by taking the difference between the observed flux and the model SED flux (the latter corresponding to the in-band stellar flux, computed by convolving the model SED with the 2MASS, IRAC and MIPS 24 filter responses respectively, following the description outlined in Robitaille et al. (2007)). In this case, the signal-to-noise ratio of the excesses is defined as the ratio of the excess (in mJy) to the photometric uncertainty (in mJy) of the overall flux measurement,  $(F_{\text{IRAC}} - F_{\text{phot}})/\sigma_{\text{IRAC}}$  (e.g, Rhee et al. 2007).  $\sigma_{\text{IRAC}}$  includes both the photometric uncertainty listed in the GLIMPSE catalog and an absolute calibration uncertainty of 5% for all IRAC bands. For the 24  $\mu\text{m}$  points we have assumed a  $\sigma_{\text{MIPS}}$  of 10% - a rather conservative value given the 4% absolute calibration uncertainty listed in the MIPS Data Handbook Version 3.3.1 but similar to the value used by Uzpen et al. (2007).

Table 7 lists the derived infrared excess fluxes above the reference stellar photosphere for the seventeen 8  $\mu\text{m}$  excess stars, along with other quantities such as the  $r'$  extinction,  $A_{r'}$ , and spectrophotometric distances  $d$ . These distances were derived from the observed  $r'$  magnitudes, corrected for the  $r'$  band extinction,  $A_{r'}$ , assuming that the absolute  $r'$  magnitude is  $M_{r'} = 1.55$  (Houk et al. 1997).

The choice of a representative A-type spectral type has a significant effect on the derived distance and extinction, while it has little effect on the derived excess flux and corresponding SNR (less than 1% change in the derived excess flux when assuming spectral types ranging from A0V to A5V spectral). In order to account for this effect,  $A_{r'}$  and  $d$  for each star were calculated assuming all possible spectral types (A0-5) and the rms value added quadratically to the  $1-\sigma$  formal uncertainties to give the errors listed in Table 6. The mid-IR excess fluxes determined for the 17 stars are listed in Table 7, where only excesses detected with a S/N higher than 3.0 are shown, consistent with the selection criteria applied over the E[K-8] distribution.

The observed SEDs are assumed to be the sum of the model stellar atmosphere SED ( $SED_{\star}$ ) and a cooler black body of a given temperature ( $SED_{\text{disk}}$ ), i.e.  $SED_{\text{tot}} = SED_{\star} + SED_{\text{disk}}$ . For each of the 17 stars in Table 7, we searched for the model that minimized the chi-squared ( $\chi^2$ ) difference between the modelled  $SED_{\text{tot}}$  and the observed data-points. The search was performed using the variable-metric routine Migrad of the Minuit package from CERN<sup>7</sup>. The iterative process finds simultaneously the best fit temperature of the black body and its angular diameter in the sky (corresponding to the square-root of the flux

---

<sup>7</sup><http://seal.web.cern.ch/seal/work-packages/mathlibs/minuit/home.html>



normalisation constant). Errors on individual parameters are estimated by searching the parameter space for the  $\delta\chi^2 = 1$  contour.

Table 7 lists the best-fit black body temperature derived for each of the 17 stars. Figure 7 shows the results from our black-body fitting routine for the 12 stars with an 8- $\mu\text{m}$  excess but lacking 24- $\mu\text{m}$  detections. The SEDs of the 5 stars with excesses at both 8  $\mu\text{m}$  and 24  $\mu\text{m}$  are shown in Figure 8. The dereddened optical IPHAS, 2MASS and GLIMPSE data points are plotted in blue, with photometric error-bars. The solid line in red corresponds to the reference photospheric SED normalised to the K-band flux. The pink dotted line represents our best-fit black-body and the solid green line represents the resulting best-fitting  $SED_{tot}$ . The optical data points were excluded from the fitting routine. For the stars lacking 24- $\mu\text{m}$  detections, the derived color temperatures provide upper limits to the maximum temperatures of the disks, as the lack of longer wavelength measurements provides no constraints on the presence of cooler material (allowing for the possibility that the parent planetesimal belts are extended over a range of radii). Nonetheless, the derived color temperatures can be used to estimate the fractional bolometric infrared fluxes due to the warm components,  $L_{\text{IR}}/L_{\star} = (A_{\text{disk}}/A_{\star}) \cdot (T_{\text{disk}}/T_{\star})^4$ , where  $A_{\text{disk}}$  and  $A_{\star}$  represent the K-band normalisation factors and  $T_{\star}=9000$  K. These correspond to distance-independent, best-fit values of  $L_{\text{IR}}/L_{\star}$ , with uncertainties dependent only on the derivation of  $T_{\text{disk}}$  and  $A_{\text{disk}}$ . For stars where an excess is detected at more than one wavelength, the resulting  $L_{\text{IR}}/L_{\star}$  values are presented in the last column of Table 7.

#### 4. Discussion

We have conducted a search for A-type dwarfs, selected from the IPHAS survey, that have mid-IR excesses in the GLIMPSE and/or MIPS GAL surveys. A sample of 2692 A-type stars was extracted by cross-correlating the optical IPHAS photometry with the mid-IR *Spitzer* GLIMPSE photometry. Follow-up optical spectroscopic observations of 18 IPHAS candidate A-type stars confirmed that all were of A-type, with only one object (6%) not fitting a main sequence star template. As expected from the IPHAS color selection criteria none of the spectra showed emission-line signatures, confirming that the selected A-stars are likely to be well-established MS stars. Figure 9, left-panel, shows the magnitude distribution of the sample at both  $r'$  and 8  $\mu\text{m}$ , together with the dereddened magnitudes. After extinction corrections, both distributions overlap as expected if, as assumed, they are A-type stars. The right-panel of Figure 9, shows the derived distance distribution of the sample. Our GLIPHAS sample traces previously unexplored photometric ranges for debris disk systems, allowing one to study the incidence of mid-IR excesses at distances of 0.5–2 kpc in the Galactic

Plane. *IRAS* searches for debris disks around MS A-type stars were restricted to  $<120$  pc (Rhee et al. 2007), while *MSX* detection limits allowed A-type stars out to 200 – 1000 pc to be surveyed (Clarke et al. 2005; Uzpen et al. 2007).

For the GLIPHAS sample of 2692 IPHAS-selected candidate A stars, 17 (0.6%) were found to have 8- $\mu\text{m}$  excesses with  $S/N > 3$ . Taking into account the probable non-A-Type contamination level of  $(15 \pm 4)\%$  present in the whole sample, the excess fraction needs to be adjusted upward to  $\sim 0.7\%$ . The above fraction of stars showing warm dust excesses is notably smaller than the  $\sim 15\%$  quoted by some pre-*Spitzer* surveys for dust excesses around MS stars (Plets & Vynckier 1999; Lagrange et al. 2000) and the 13% occurrence fraction quoted by Song et al. (2001) for A-type stars with ages ranging from 50 Myr to 1 Gyr. These works, however, quantified the excess fractions at wavelengths beyond 24  $\mu\text{m}$  and therefore cannot be used for comparison. On the other hand, the dust excess fraction of 0.7% found by us at 8  $\mu\text{m}$  is similar to the fraction with dust excesses found at 12  $\mu\text{m}$  from *IRAS* searches, and coincides with *MSX* and *GLIMPSE* Galactic Plane results of Uzpen et al. (2007), who found that 4 out of 391 A-type stars in their sample (1.0%) showed 8- $\mu\text{m}$  excesses. Further, our derived fraction of warm excesses 0.7% is also consistent with the 1.2% frequency of warm excesses found in young clusters (Hernández et al. 2006; Currie et al. 2008; Uzpen et al. 2008), and with recent results from Uzpen et al. (2008) that report a 0.3% incidence fraction of warm excesses among 338 field stars.

We find that none of the 8- $\mu\text{m}$  excess sources show JHK excesses, which rules out the presence of very hot dust in the inner parts of their disks. Four objects (24%) show excesses at wavelengths shorter than 5.8  $\mu\text{m}$ , imposing strong constraints on the presence of hot dust. This supports the hypothesis that the objects in this sample are relatively evolved systems, older than T Tauri and Herbig Ae stars (as expected from the lack of  $H\alpha$  emission, given their  $(r' - H_\alpha)$  colors). Table 7 lists and Figure 10 displays the blackbody dust temperatures and  $L_{\text{IR}}/L_\star$  values for both the 8  $\mu\text{m}$  and 24  $\mu\text{m}$  excess samples. Only one object has  $T_{\text{disk}} > 500$  K within the errors. We find that the SEDs of the mid-IR excess sources can be fitted by blackbodies with temperatures ranging from 270 – 650 K (for those with detected excesses at more than one wavelength) comparable to recent samples of warm ( $T > 200$  K) excess candidates identified with *Spitzer* (Uzpen et al. 2005, 2007; Hernández et al. 2006; Currie et al. 2008).

The derived color temperatures provide only upper limits to the maximum temperatures of the disks, as the lack of longer wavelength measurements provides no constraints on the presence of cooler material (allowing for the possibility that the parent planetesimal belts are extended over a range of radii). Based on simple radiative equilibrium (e.g. Currie et al. 2008), the derived disk temperatures would imply parent planetesimal belts confined to disk

regions of  $\sim 0.8 - 10$  AU.

The mid-IR excess systems are found to have fractional disk-to-star luminosity ratios,  $L_{\text{IR}}/L_{\star}$ , ranging from  $2.2 \times 10^{-3} - 1.9 \times 10^{-2}$ , with a mean of  $7.9 \times 10^{-3}$ . But since cooler dust emitting at far-IR wavelengths may also be present around the above  $L_{\text{IR}}/L_{\star}$  values are strictly only lower limits. However, for systems with detectable mid-IR excesses for which longer wavelength data are also available (e.g. the sample of Sylvester et al. (1996)), most of the excess luminosity appears at the shorter wavelengths. The range of fractional luminosities found here are in between the values expected for luminous debris-disk and evolved T Tauri and Herbig Ae/Be systems with cleared inner regions.

The low incidence rate of mid-IR excesses found in our survey is consistent with previous inferences that the inner regions of CS disks are cleared faster than the outer regions, resulting in a greater persistence of long wavelength excesses (Hayashi et al. 1985; Backman & Paresce 1993; Meyer et al. 2007; Cieza et al. 2007). Most prior examples of stars with 8-12  $\mu\text{m}$  excesses had  $\text{H}\alpha$  emission as well as near-IR excesses, e.g. as found by Dunkin et al. (1997) for the Sylvester et al. (1996) sample of A-stars with mid-IR excesses; our stars, with no net  $\text{H}\alpha$  emission and no noticeable near-IR excesses, are likely to be only a little older than those stars with  $\text{H}\alpha$  emission that show 8-12  $\mu\text{m}$  excesses. Our IPHAS color-selection method ensures the great preponderance of selected stars will be older than 10 Myr (as described by Drew et al. 2008), whilst stars in the age range 5-10 Myrs are admitted as their  $\text{H}\alpha$  emission becomes insignificant. The very small proportion (0.7%) of near-MS A stars found to exhibit disk emission at 8  $\mu\text{m}$  are most likely at the younger end of the entire sample of A stars that have debris disks. Currie et al. (2008) found that the fraction of true debris-disks ( $L_{\text{IR}}/L_{\star} \ll 10^{-3}$ ) peaks at 10-15 Myr, consistent with the low fraction of warm,  $\beta$  Pictoris-like, debris-disks identified in this work.

The identification and detailed study of systems with intermediate values of  $L_{\text{IR}}/L_{\star}$  ( $10^{-3} - 10^{-2}$ ) is crucial in order to fully understand the disk-clearing and planet formation processes. Here we have exploited the current generation of photometric Galactic surveys to increase substantially the number of known mid-IR excess A-type MS systems, which are likely to be at this evolutionary stage. High-resolution spectroscopic follow-up observations of the sample should be carried out in order to refine the stellar properties (surface gravity, rotational velocities and metallicities), allowing them to be placed within the context of other known samples of debris disks.

## 5. Conclusions

Using results from the IPHAS, GLIMPSE and MIPS GAL Galactic Plane surveys, we have identified 17 new main sequence A-type systems with warm excesses at  $8\ \mu\text{m}$  and/or  $24\ \mu\text{m}$ . Optical classification spectra obtained of 10 of the systems confirmed that all but one were main sequence A-type stars, the exception being an A5Ia supergiant. The systems have bolometric excess ratios comparable to those of warm debris-disk systems, similar to  $\beta$  Pictoris. The overall fraction of sources with  $8\ \mu\text{m}$  excesses was found to be 0.7 %. The identification of these new CS disk systems shows the potential of new surveys to increase substantially our knowledge of the occurrence and characteristics of CS disks in transition between their primordial and debris-disk phases. When both the IPHAS and MIPS GAL surveys are complete, an analysis of the full data-sets is planned in order to provide a more complete sample of Galactic Plane main sequence A-type debris disk stars.

## Acknowledgments

This work was based partially on observations made with the Isaac Newton Telescope and the William Herschel Telescopes, which are operated by the Isaac Newton Group in the Observatorio del Roque de los Muchachos of the Instituto de Astrofísica de Canarias, La Palma, Spain. IPHAS observing time was made available by the time allocation committees of the UK, Spain and The Netherlands. The WHT ISIS spectra were obtained as part of the 2006/7 International Time Programme: ‘An IPHAS-based exploration of stellar populations in the northern Milky Way’. This work made use of data products from the GLIMPSE survey, which is a legacy science program of the *Spitzer Space Telescope*, funded by the National Aeronautics and Space Administration; of the SIMBAD database and other facilities operated at CDS, Strasbourg, France; and of the 2MASS point-source catalog available at the NASA/IPAC Infrared Science Archive, which is operated by the Jet Propulsion Laboratory, California Institute of Technology, under contract with the National Aeronautics and Space Administration. ASH carried out part of this work whilst being funded by the PPARC Gemini - Fundación Andes UK/Chile studentship programme. Parts of the analysis presented here made use of the Perl Data Language (PDL), which can be obtained from [www.perl.org](http://www.perl.org).

Table 1. Summary of processed IPHAS object catalogs

Field ID	l [deg]	b [deg]	RA	DEC	Seeing [arcsec]	Total Stars	Total A-type dwarfs	Total with GLIMPSE Correlations
4205	29.58	-0.80	18:48:8.94	-03:21:0.0	0.9	874	138	0
4188	29.73	-0.30	18:46:40.25	-02:59:0.0	1.5	0	179	3
4213	30.15	-0.71	18:48:53.05	-02:48:0.0	1.1	612	50	36
4196	30.31	-0.21	18:47:24.49	-02:26:0.0	1.1	942	175	158
4222	30.72	-0.62	18:49:37.12	-02:15:0.0	1.0	589	67	60
4189	31.04	0.37	18:46:40.62	-01:31:0.0	1.5	1698	136	125
4254	31.14	-1.03	18:51:49.68	-02:04:0.0	1.3	1425	175	85
4232	31.30	-0.53	18:50:21.29	-01:42:0.0	1.0	2737	214	182
4214	31.45	-0.04	18:48:53.12	-01:20:0.0	1.0	2548	359	292
4197	31.61	0.45	18:47:25.01	-00:58:0.0	1.0	2043	191	63
4265	31.71	-0.94	18:52:33.68	-01:31:0.0	1.5	4327	211	148
4242	31.87	-0.45	18:51:05.41	-01:09:0.0	1.3	4059	388	265
4223	32.03	0.05	18:49:37.33	-00:47:0.0	1.3	3246	423	0
4206	32.19	0.54	18:48:09.30	-00:25:0.0	1.0	1183	97	1
4275	32.28	-0.85	18:53:17.65	-00:58:0.0	1.3	5864	351	104
4190	32.35	1.03	18:46:41.45	-00:03:0.0	1.3	1570	125	6
4253	32.44	-0.36	18:51:49.47	-00:36:0.0	1.3	4314	538	0
4233	32.60	0.13	18:50:21.48	-00:14:0.0	1.1	2286	306	18
4215	32.76	0.63	18:48:53.54	00:08:0.0	1.1	1164	103	90
4285	32.86	-0.77	18:54:01.56	-00:25:0.0	1.5	7301	501	0
4263	33.02	-0.27	18:52:33.49	-00:03:0.0	1.4	3737	389	111
4243	33.17	0.22	18:51:05.58	00:19:0.0	1.3	1170	131	112
4297	33.43	-0.68	18:54:45.46	00:08:0.0	1.3	4000	541	377
4274	33.59	-0.18	18:53:17.57	00:30:0.0	1.3	1058	79	77
4255	33.75	0.31	18:51:49.73	00:52:0.0	1.3	885	62	53
4235	33.91	0.80	18:50:22.03	01:14:0.0	1.2	596	55	43
4309	34.00	-0.59	18:55:29.42	00:41:0.0	1.1	935	75	66
4286	34.16	-0.10	18:54:01.61	01:03:0.0	1.4	637	63	58
4266	34.32	0.40	18:52:33.84	01:25:0.0	1.5	837	82	67
4348	34.42	-1.00	18:57:41.24	00:52:0.0	1.3	343	17	14
4246	34.48	0.89	18:51:06.18	01:47:0.0	1.2	549	34	33
4322	34.58	-0.50	18:56:13.36	01:14:0.0	1.2	835	55	48
4298	34.73	-0.01	18:54:45.60	01:36:0.0	1.3	961	94	86
4276	34.89	0.48	18:53:17.88	01:58:0.0	1.0	464	31	28
4361	34.99	-0.91	18:58:25.07	01:25:0.0	1.3	903	27	17
4256	35.05	0.97	18:51:50.27	02:20:0.0	1.2	370	40	26
4334	35.15	-0.41	18:56:57.25	01:47:0.0	1.3	779	41	30
4288	35.47	0.57	18:54:01.88	02:31:0.0	1.5	451	50	49
4299	36.04	0.66	18:54:45.84	03:04:0.0	1.6	717	85	81
4336	36.45	0.26	18:56:57.35	03:15:0.0	1.3	313	28	28
4401	36.71	-0.64	19:00:36.45	03:04:0.0	1.3	706	72	69
4325	37.19	0.84	18:56:13.71	04:10:0.0	1.5	210	14	14
4415	37.28	-0.55	19:01:20.27	03:37:0.0	1.6	362	44	43
4388	37.44	-0.06	18:59:52.68	03:59:0.0	1.5	333	34	34
4402	38.01	0.03	19:00:36.50	04:32:0.0	1.5	278	16	15
4417	38.58	0.12	19:01:20.30	05:05:0.0	1.5	439	24	24
4389	38.74	0.61	18:59:52.75	05:27:0.0	1.5	325	24	23
4459	39.00	-0.28	19:03:31.64	05:16:0.0	1.6	679	76	74
4403	39.32	0.70	19:00:36.52	06:00:0.0	1.4	565	36	33
4504	39.41	-0.68	19:05:42.97	05:27:0.0	1.4	1073	102	99
4473	39.57	-0.19	19:04:15.41	05:49:0.0	1.4	647	58	57
4416	39.89	0.79	19:01:20.28	06:33:0.0	1.5	817	50	40
4488	40.14	-0.10	19:04:59.19	06:22:0.0	1.5	1008	129	92
4458	40.30	0.39	19:03:31.62	06:44:0.0	1.7	1310	154	147
4534	40.55	-0.50	19:07:10.52	06:33:0.0	1.4	1059	97	91
4503	40.71	-0.01	19:05:42.95	06:55:0.0	1.1	1176	104	100
4518	41.28	0.09	19:06:26.71	07:28:0.0	1.1	1213	82	80
4593	41.54	-0.80	19:10:05.70	07:17:0.0	1.1	903	73	72
4533	41.85	0.18	19:07:10.48	08:01:0.0	1.6	986	78	70
4502	42.01	0.67	19:05:42.78	08:23:0.0	1.2	1010	111	109
4609	42.11	-0.71	19:10:49.52	07:50:0.0	1.5	773	46	30
4517	42.59	0.76	19:06:26.46	08:56:0.0	1.2	1005	80	78
4624	42.68	-0.61	19:11:33.34	08:23:0.0	1.5	1130	69	65
4592	42.84	-0.12	19:10:05.66	08:45:0.0	1.2	880	46	40
4532	43.16	0.85	19:07:10.12	09:29:0.0	1.2	2106	248	210
4607	43.41	-0.03	19:10:49.45	09:18:0.0	1.5	799	94	82

Table 1—Continued

Field ID	l [deg]	b [deg]	RA	DEC	Seeing [arcsec]	Total Stars	Total A-type dwarfs	Total with GLIMPSE Correlations
4682	43.66	-0.91	19:14:28.73	09:07:0.0	1.5	2782	150	123
4623	43.98	0.07	19:11:33.25	09:51:0.0	1.3	1125	107	69
4590	44.14	0.55	19:10:05.41	10:13:0.0	1.1	2153	335	314
4699	44.24	-0.82	19:15:12.66	09:40:0.0	1.6	1366	99	89
4605	44.71	0.65	19:10:49.07	10:46:0.0	1.5	3485	436	381
4714	44.81	-0.72	19:15:56.63	10:13:0.0	1.5	1469	136	118
4683	44.96	-0.23	19:14:28.75	10:35:0.0	1.6	1696	151	84
4620	45.28	0.75	19:11:32.73	11:19:0.0	1.2	4395	392	325
4665	45.69	0.35	19:13:44.59	11:30:0.0	1.5	1122	167	156
4635	45.85	0.84	19:12:16.41	11:52:0.0	1.2	4230	584	334
4679	46.26	0.45	19:14:28.38	12:03:0.0	1.2	1321	265	258
4649	46.42	0.94	19:12:59.97	12:25:0.0	1.7	2946	380	209
4802	46.93	-0.82	19:20:20.63	12:03:0.0	1.7	1464	146	99
4663	46.99	1.04	19:13:43.53	12:58:0.0	1.6	1943	191	76
4817	47.50	-0.72	19:21:04.70	12:36:0.0	1.8	1043	93	88
4831	48.07	-0.62	19:21:48.80	13:09:0.0	1.8	1792	22	18
4801	48.23	-0.13	19:20:20.42	13:31:0.0	1.8	1927	212	195
4816	48.80	-0.03	19:21:04.48	14:04:0.0	1.8	2088	184	155
4859	49.21	-0.42	19:23:17.20	14:15:0.0	1.6	1736	165	151
4830	49.36	0.07	19:21:48.57	14:37:0.0	1.8	1660	5	0
4902	49.63	-0.80	19:25:30.00	14:26:0.0	1.8	2419	199	184
4916	50.19	-0.70	19:26:14.31	14:59:0.0	0.9	2174	233	218
4857	50.50	0.28	19:23:16.58	15:43:0.0	1.6	1983	143	133
4930	50.76	-0.59	19:26:58.69	15:32:0.0	0.9	2331	92	80
4901	50.92	-0.10	19:25:29.72	15:54:0.0	1.6	1983	120	112
4973	51.18	-0.97	19:29:11.95	15:43:0.0	0.9	1460	142	93
4944	51.33	-0.49	19:27:43.14	16:05:0.0	1.1	1946	118	109
4915	51.48	0.00	19:26:14.02	16:27:0.0	0.9	2384	236	228
4986	51.75	-0.87	19:29:56.62	16:16:0.0	0.9	1695	59	55
4928	52.05	0.11	19:26:58.16	17:00:0.0	0.9	1984	255	139
4899	52.20	0.60	19:25:28.54	17:22:0.0	1.7	1995	156	139
5000	52.32	-0.76	19:30:41.19	16:49:0.0	1.3	2357	207	196
4972	52.47	-0.27	19:29:11.83	17:11:0.0	1.2	1283	86	82
4942	52.62	0.22	19:27:42.38	17:33:0.0	0.9	1687	118	112
4912	52.77	0.70	19:26:12.55	17:55:0.0	0.9	2044	190	162
5015	52.88	-0.65	19:31:25.81	17:22:0.0	1.2	2380	174	124
4985	53.03	-0.16	19:29:56.29	17:44:0.0	0.9	1008	35	35
4926	53.34	0.81	19:26:56.63	18:27:59.9	0.9	2075	147	130
4999	53.60	-0.05	19:30:40.82	18:17:0.0	1.3	1364	118	111
4970	53.75	0.43	19:29:10.98	18:38:59.9	1.6	1694	171	138
4939	53.90	0.92	19:27:40.50	19:00:59.9	1.1	3148	402	299
5014	54.17	0.06	19:31:25.45	18:49:59.9	1.3	3285	324	219
4983	54.32	0.54	19:29:55.14	19:11:59.9	0.9	5067	188	88
4997	54.89	0.66	19:30:39.36	19:44:59.9	1.3	5019	436	192
5098	55.00	-0.70	19:35:54.90	19:11:59.9	0.9	3108	287	108
5069	55.15	-0.21	19:34:24.73	19:33:59.9	0.8	4650	400	224
5041	55.30	0.28	19:32:54.41	19:55:59.9	0.9	4928	183	98
5112	55.57	-0.58	19:36:39.94	19:44:59.9	1.1	4229	619	397
5083	55.72	-0.09	19:35:09.55	20:06:59.9	0.9	4422	561	379
5025	56.02	0.88	19:32:08.01	20:50:59.9	1.1	2828	60	30
5126	56.14	-0.47	19:37:25.09	20:17:59.9	0.9	4457	399	240
5097	56.28	0.02	19:35:54.46	20:39:59.9	0.9	2286	139	131
5039	56.58	1.00	19:32:52.14	21:23:59.9	0.9	2723	190	112
5140	56.70	-0.35	19:38:10.34	20:50:59.9	1.6	2467	198	186
5111	56.85	0.14	19:36:39.48	21:12:59.9	1.0	1207	70	67
5080	57.00	0.62	19:35:08.16	21:34:59.9	0.8	1734	168	53
5124	57.41	0.25	19:37:24.30	21:45:59.9	1.0	689	79	78
5095	57.56	0.74	19:35:52.71	22:07:59.9	0.9	1645	102	97
5138	57.98	0.37	19:38:09.21	22:18:59.9	1.5	1558	85	47
5108	58.13	0.86	19:36:37.36	22:40:59.9	0.9	2288	178	106
5152	58.54	0.49	19:38:54.23	22:51:59.9	1.5	1867	133	106
5262	59.24	-0.73	19:45:00.13	22:51:59.9	1.1	3095	240	221
5277	59.80	-0.61	19:45:45.96	23:24:59.9	1.1	2592	207	195
5261	60.51	0.01	19:44:59.57	24:19:59.9	1.3	4143	413	341
5275	61.07	0.13	19:45:45.38	24:52:59.9	1.1	3989	387	261
5273	62.33	0.88	19:45:42.67	26:20:59.8	1.1	2978	246	194

Table 1—Continued

Field ID	l [deg]	b [deg]	RA	DEC	Seeing [arcsec]	Total Stars	Total A-type dwarfs	Total with GLIMPSE Correlations
5285	62.89	1.01	19:46:27.69	26:53:59.8	1.0	4273	288	116
5489	65.02	-0.76	19:58:11.41	27:48:59.8	1.5	2900	196	74
TOTAL						260223	23050	15312

Table 2. Survey observational properties

Filter	Central wavelength [ $\mu\text{m}$ ]	Zeropoint [Jy]	FWHM [arcseconds]	Lower flux limits [mJy/mag]
IPHAS $r'$	0.624	3173.3	< 2.0	0.2/18
IPHAS $i'$	0.774	2515.7	< 2.0	0.02/20.5
IPHAS $H\alpha$	0.656	2974.4	< 2.0	0.02/20.5
2MASS J	1.235	1594.5	$\sim 3.1$	0.7/15.8
2MASS H	1.662	1024.5	$\sim 3.0$	0.9/15.1
2MASS K	2.159	666.7	$\sim 3.1$	1.2/14.3
GLIMPSE IRAC 1	3.550	277.5	1.6	0.6/14.2
GLIMPSE IRAC 2	4.493	179.5	1.7	0.4/14
GLIMPSE IRAC 3	5.731	116.5	1.8	2/11.9
GLIMPSE IRAC 4	7.872	63.1	1.9	10/9.5
MIPSGAL MIPS 1	23.670	7.13	5.5	1/9.6

Note. — Filter characteristics, spatial resolution and photometric sensitivities of the IPHAS, 2MASS, GLIMPSE and MIPSGAL 24- $\mu\text{m}$  surveys. Note that the GLIMPSE catalog includes sources with fluxes smaller than these sensitivities, provided they have a  $\text{SN} > 3$  and that they meet the 2+1 criterion in the other bands. The zeropoint (luminosity of a 0th magnitude star) in each band is given for conversion from fluxes to magnitudes. From Drew et al. (2005), Cutri et al. (2003), the *Spitzer* Observer Manual Version 7.1, the GLIMPSE Legacy Data Products Notes version 2.0 and the Infrared Processing and Analysis Center (IPAC).

Table 3. Source counts and mean observed magnitude for the IPHAS-GLIMPSE sample of A-type stars

Band	Number of stars	Mean observed magnitude
$r'$	15312	16.179
$i'$	15312	14.892
J	12748	14.045
H	12485	13.546
K	11198	13.281
3.6	11175	12.982
4.5	11037	12.969
5.8	5111	12.385
8	2751	12.097



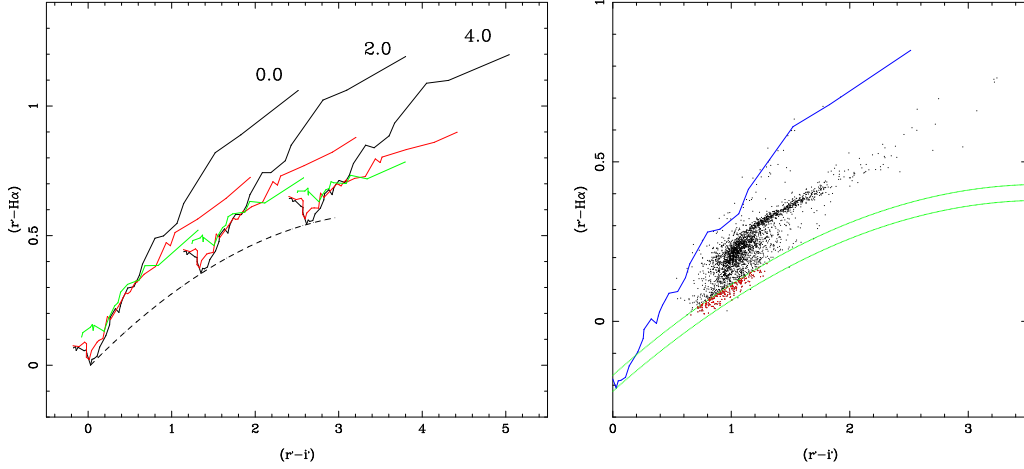


Fig. 1.— *Left-hand panel:* Synthetic  $(r' - H_\alpha)$  versus  $(r' - i')$  colors of normal stars under the effect of interstellar extinction (adapted from Drew et al. (2005)). For a given visual color excess  $E(B - V)$ , the black lines represent the main sequence, the red lines represent the giant sequence and the green lines show the positions of the supergiants. The dashed line shows the reddening track for the normal metallicity A0V star from the Pickles (1998) library: it is a representative early-A reddening line. *Right-hand panel:* The  $(r' - H_\alpha)$  versus  $(r' - i')$  color plane for IPHAS field 4232. An *early-A* star strip, of width 0.05 mags in  $(r' - H_\alpha)$  (green lines) was used to select for A-type dwarfs (red dots). The blue line corresponds to an unreddened MS track.

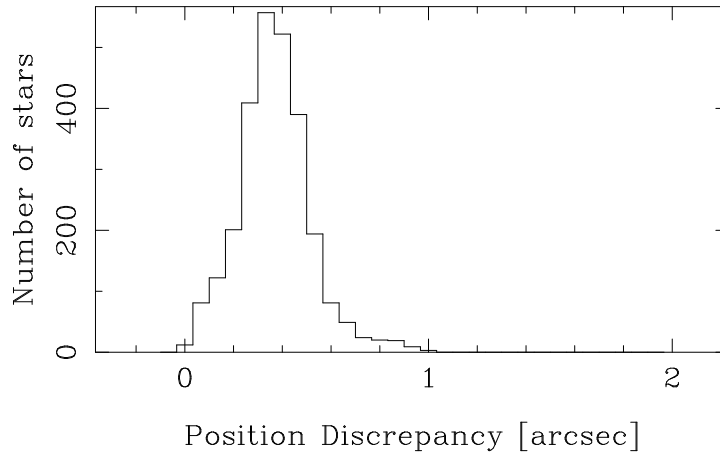


Fig. 2.— Distributions of radial distances between the IPHAS and GLIMPSE positions.

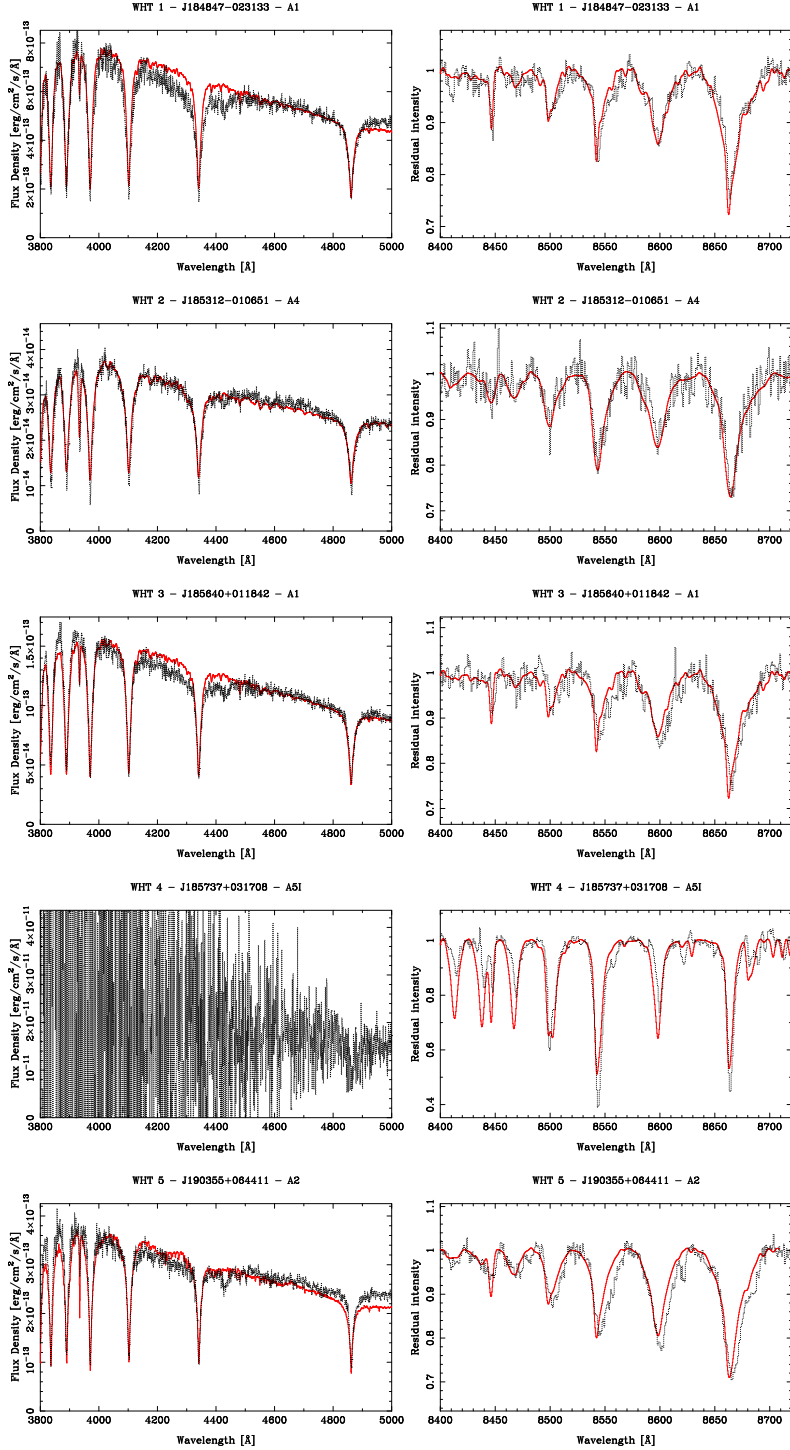


Fig. 3.— WHT ISIS Spectra of IPHAS-selected A-type stars. The dereddened flux-calibrated spectra of the targets (black dotted lines) are shown for the blue spectral region (left-hand panels) and for the red spectral region (right-hand panels), and are compared to the spectra of the A-type spectral standards that provide the best match to their red spectral features (red solid lines). The spectral subtypes of these spectral standards are shown at the top of each plot. All of the plotted spectral standards are luminosity class V dwarfs, except for WHT 4, which is best matched by an A5Ia supergiant spectrum.

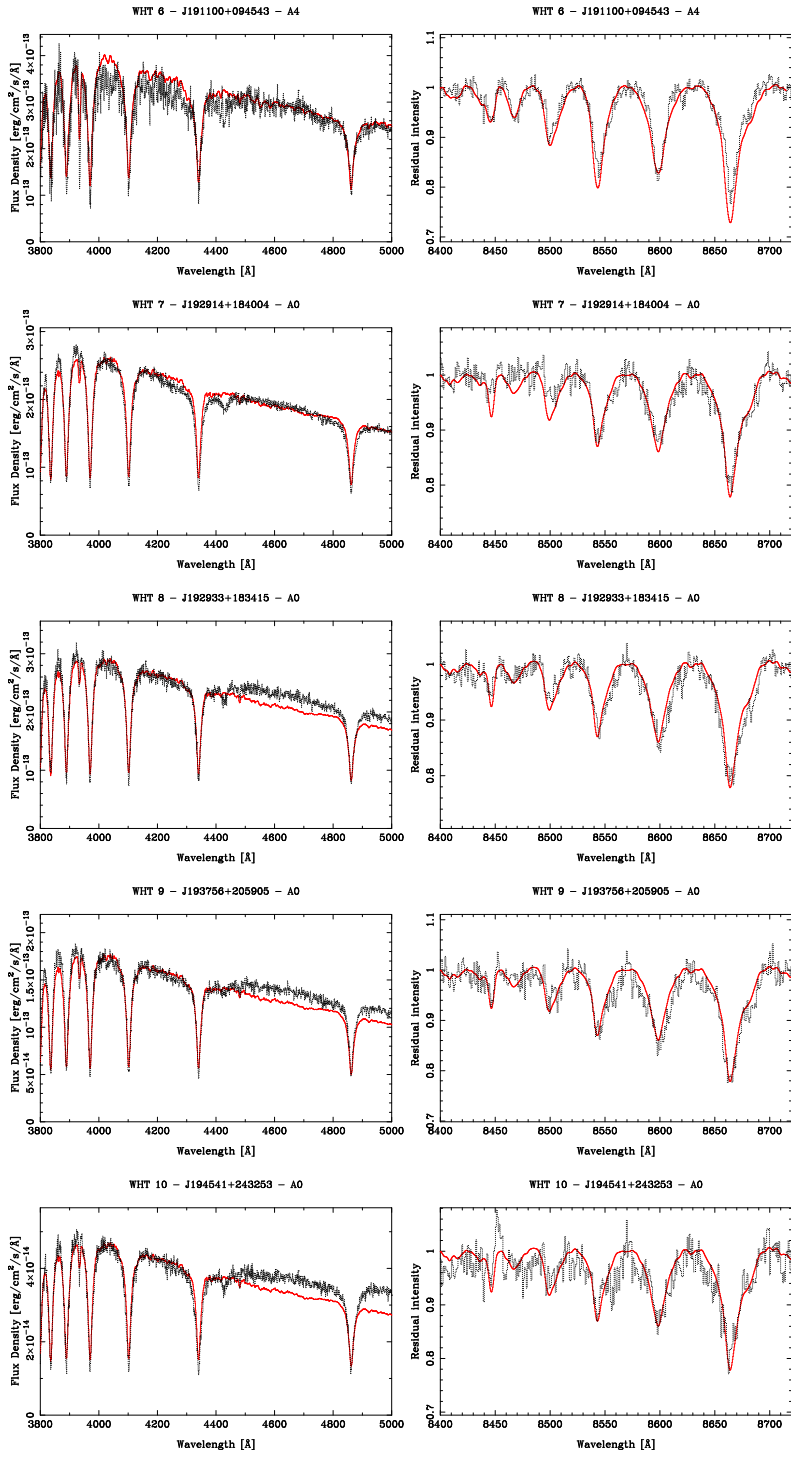


Fig. 3.— *continued*

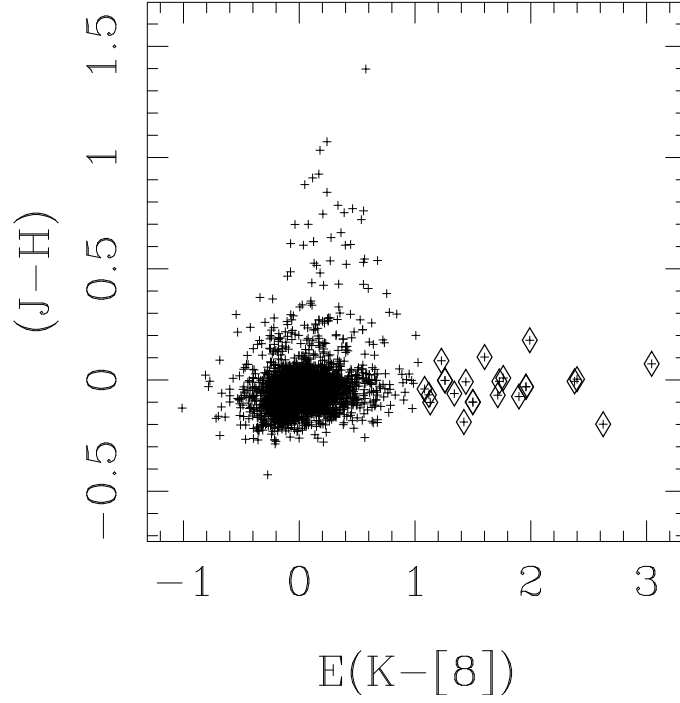


Fig. 4.— Dereddened  $(J - H) - (K - 8)$  color-color diagram for the 2692 A-type stars in the GLIPHAS sample. The 20 objects having a  $(K - 8)$  color excess with  $\text{SN} > 3$  are highlighted with diamond symbols.

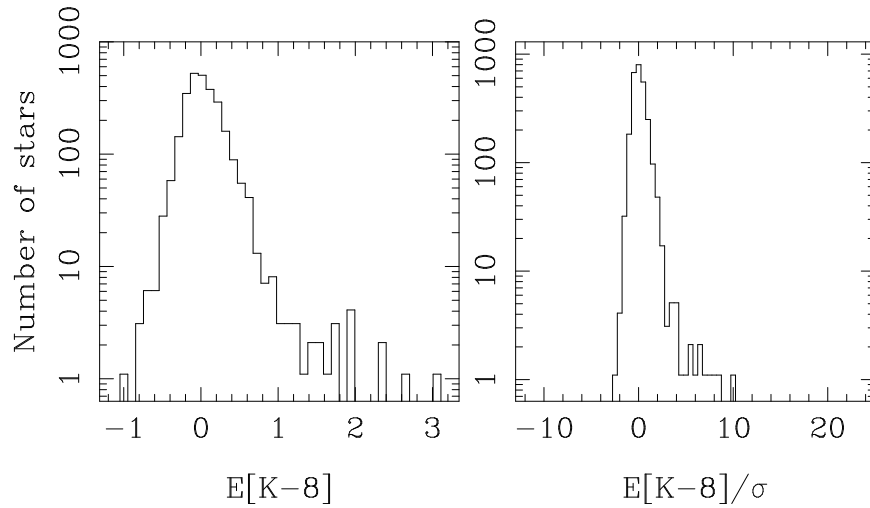


Fig. 5.— *Left-hand panel:* Distributions of  $E(K - 8)$  color excesses for 2692 A-type stars in the GLIPHAS sample. *Right-hand panel:* Distributions of signal-to-noise for  $(K - 8)$  color excesses.

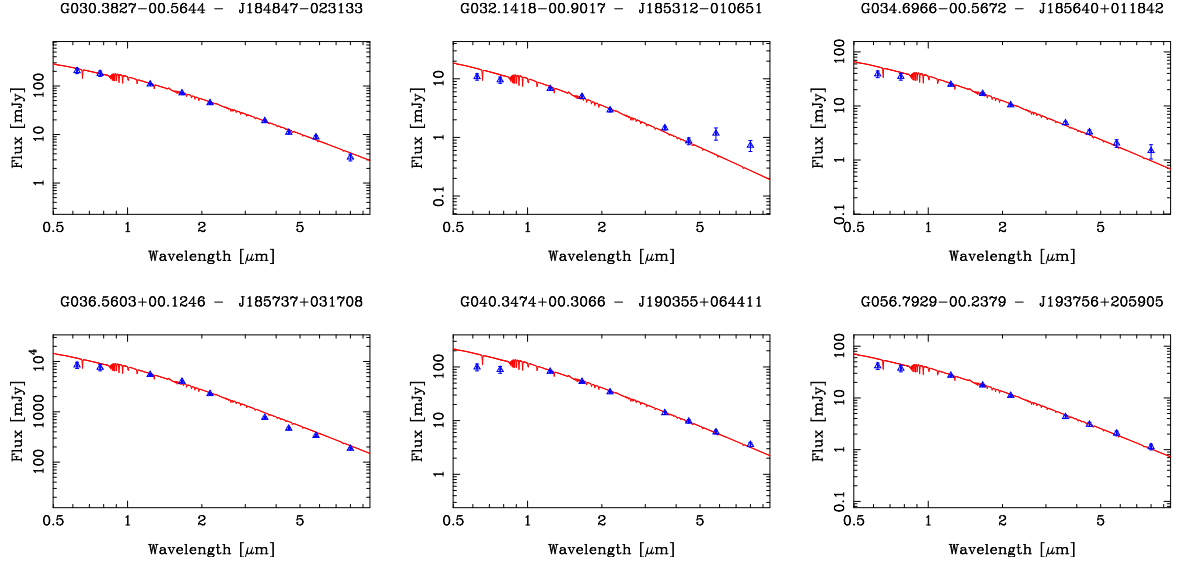


Fig. 6.— Dereddened optical IPHAS, 2MASS and GLIMPSE photometry for the 6 WHT A-type stars with no evidence of 8- $\mu$ m excesses (blue triangles with error bars denoting the  $1\sigma$  photometric error of each measurement). For each star, the red solid line corresponds to the photospheric reference of an A3V SED, normalised to the K-band flux.

Table 4. WHT/ISIS Spectral Classifications

Star	Red-based	Blue-Based	8498.02 Å	Ca II EW's (Å)		
				8542.09 Å	8662.14 Å	3933.663 Å
WHT1 - J184847-023133	A1V	A1V	0.64(0.21)	1.71(0.27)	3.65(0.32)	1.36(0.31)
WHT2 - J185312-010651	A4V	A6V	0.91(0.32)	1.83(0.39)	4.39(0.31)	1.44(0.42)
WHT3 - J185640+011842	A1V	A2V	0.52(0.25)	3.02(0.29)	4.87(0.39)	0.87(0.21)
WHT4 - J185737+031708	A5Ia	-	2.76(0.32)	5.48(0.41)	4.41(0.37)	-
WHT5 - J190355+064411	A2V	A3V	1.33(0.19)	2.95(0.22)	6.17(0.29)	1.08(0.21)
WHT6 - J191100+094543	A4V	A7V	1.15(0.34)	2.36(0.31)	4.09(0.32)	3.34(0.37)
WHT7 - J192914+184004	A0V	A0V	0.36(0.17)	1.44(0.21)	4.41(0.27)	0.61(0.19)
WHT8 - J192933+183415	A0V	A0V	0.33(0.17)	1.72(0.23)	4.55(0.28)	0.44(0.24)
WHT9 - J193756+205905	A0V	A2V	0.49(0.19)	1.68(0.24)	4.31(0.33)	1.05(0.25)
WHT10 - J194541+243253	A0V	A2V	0.25(0.19)	1.51(0.34)	3.36(0.41)	1.08(0.33)

Note. — Blue- (Ca II K) and red-based (Ca II IR-triplet) spectral classifications for stars observed with the WHT. The red-based spectral types are 0.9 sub-types earlier on average than the blue-based ones (see text). The measured equivalent widths of the Ca II-K and IR-triplet lines are given in Å, with the numbers in brackets denoting the  $2\sigma$  uncertainties.

Table 5. Photometry for GLIPHAS A-type stars with WHT spectra but with no 8- $\mu$ m excesses

WHT No.	IPHAS ID	$r'$ (mag)	$r'-i'$ (mag)	J (mag)	J-H (mag)	J-K (mag)	J-[3.6] (mag)	[3.6] (mag)	[3.6]-[4.5] (mag)	[3.6]-[5.8] (mag)	[3.6]-[8.0] (mag)	$A_{r'}$ (mag)	d (kpc)
1	J184847-023133	14.48(0.02)	1.09(0.03)	11.69(0.02)	0.44(0.03)	0.70(0.03)	0.97(0.05)	10.72	-0.05(0.08)	0.18(0.09)	0.79(0.08)	4.1 (0.3)	0.6 (0.1)
2	J185312-010651	15.70(0.01)	0.57(0.01)	14.00(0.05)	0.32(0.08)	0.35(0.09)	0.65(0.09)	13.35	-0.05(0.16)	0.75(0.26)	0.90(0.24)	2.0 (0.2)	2.6 (0.5)
3	J185640+011842	14.71(0.02)	0.76(0.03)	12.85(0.02)	0.33(0.03)	0.47(0.04)	0.75(0.06)	12.10	0.10(0.12)	0.45(0.13)	0.93(0.20)	2.8 (0.3)	1.2 (0.2)
4	J185737+031708	15.19(0.01)	2.38(0.01)	9.18(0.02)	1.13(0.05)	1.70(0.03)	2.05(0.04)	7.13	0.10(0.05)	0.21(0.05)	0.24(0.04)	9.1 (0.2)	0.1 (0.0)
5	J190355+064411	14.24(0.04)	0.90(0.06)	11.74(0.02)	0.34(0.04)	0.57(0.03)	0.74(0.07)	11.00	0.14(0.09)	0.11(0.10)	0.53(0.09)	3.3 (0.3)	0.7 (0.2)
9	J193756+205905	14.46(0.02)	0.71(0.03)	12.70(0.02)	0.27(0.03)	0.42(0.03)	0.49(0.05)	12.21	0.15(0.10)	0.19(0.12)	0.78(0.09)	2.6 (0.3)	1.1 (0.2)

Note. — Observed magnitudes and colors in the different IPHAS, 2MASS and IRAC bands, together with visual extinctions,  $A_{r'}$ , and spectrophotometric distances derived from the IPHAS colors. The figures in brackets denote the  $1\sigma$  uncertainties. For each star, extinctions and distances were computed assuming all possible spectral types (A0-5), and the rms value of each quantity was added quadratically to the photometric errors to derive the final uncertainties quoted here.

Table 6. Photometry for IPHAS A-type stars with 8- $\mu$ m excesses

GLIPHAS No.	IPHAS ID	r' (mag)	r'-i' (mag)	r'-J (mag)	J (mag)	J-H (mag)	J-K (mag)	J-[3.6] (mag)	[3.6] (mag)	[3.6]-[4.5] (mag)	[3.6]-[5.8] (mag)	[3.6]-[8.0] (mag)	[24] (mag)
1	J190602+073418	15.20(0.02)	1.07(0.03)	2.16(0.03)	13.04(0.02)	0.40(0.04)	0.57(0.04)	0.73(0.06)	12.31	0.10(0.12)	0.10(0.14)	1.30(0.11)	7.93 0.11
2	J190650+090108	16.89(0.01)	1.60(0.01)	3.44(0.03)	13.45(0.03)	0.57(0.04)	0.91(0.05)	1.18(0.11)	12.27	0.46(0.17)	0.27(0.16)	2.84(0.18)	<
3	J190952+070514	17.41(0.02)	1.45(0.02)	3.80(0.03)	13.61(0.02)	0.62(0.03)	0.93(0.03)	1.33(0.06)	12.28	-0.37(0.14)	0.06(0.17)	1.94(0.29)	<
4	J191100+094543	15.18(0.01)	1.18(0.02)	3.00(0.02)	12.18(0.02)	0.57(0.03)	1.04(0.03)	1.98(0.04)	10.20	0.55(0.07)	1.05(0.06)	1.82(0.05)	7.06 0.11
5	J191512+120907	17.54(0.04)	1.19(0.05)	2.89(0.06)	14.65(0.05)	0.58(0.07)	0.82(0.08)	0.89(0.08)	13.76	0.07(0.17)	1.13(0.25)	2.06(0.14)	<
6	J191947+132707	17.82(0.00)	1.30(0.01)	3.33(0.03)	14.49(0.03)	0.62(0.07)	0.95(0.09)	0.97(0.08)	13.52	0.23(0.18)	2.28(0.18)	2.76(0.15)	<
7	J192227+141309	14.83(0.04)	0.95(0.05)	2.35(0.04)	12.48(0.02)	0.34(0.04)	0.55(0.03)	0.82(0.06)	11.66	0.02(0.09)	0.65(0.18)	1.52(0.33)	<
8	J192612+163544	16.87(0.03)	0.94(0.04)	2.44(0.04)	14.43(0.03)	0.37(0.05)	0.72(0.06)	0.82(0.10)	13.61	0.08(0.17)	0.62(0.32)	1.31(0.24)	<
9	J192914+184004	14.53(0.02)	0.85(0.03)	2.12(0.03)	12.41(0.02)	0.36(0.03)	0.52(0.03)	0.68(0.05)	11.73	0.33(0.09)	0.66(0.10)	2.06(0.07)	6.40 0.11
10	J192933+183415	14.15(0.01)	0.68(0.01)	1.81(0.02)	12.34(0.02)	0.42(0.03)	0.77(0.03)	1.28(0.06)	11.06	0.19(0.07)	0.38(0.08)	1.29(0.06)	7.61 0.10
11	J193110+164225	17.54(0.00)	1.35(0.01)	3.22(0.03)	14.32(0.03)	0.45(0.05)	0.79(0.04)	0.95(0.07)	13.37	0.14(0.14)	0.98(0.27)	1.67(0.19)	<
12	J193117+185048	17.34(0.03)	1.13(0.04)	2.79(0.04)	14.55(0.03)	0.46(0.05)	0.57(0.06)	1.04(0.08)	13.51	0.24(0.15)	1.22(0.16)	1.59(0.17)	<
13	J193126+184131	15.74(0.00)	0.99(0.01)	2.48(0.02)	13.26(0.02)	0.47(0.03)	0.79(0.03)	0.82(0.06)	12.44	0.05(0.11)	0.56(0.14)	1.53(0.18)	<
14	J193259+195709	16.77(0.02)	1.08(0.03)	2.65(0.03)	14.12(0.02)	0.59(0.03)	0.95(0.03)	1.55(0.09)	12.57	0.22(0.15)	1.12(0.14)	2.78(0.12)	<
15	J193516+195803	15.97(0.00)	0.77(0.01)	1.94(0.02)	14.03(0.02)	0.34(0.04)	0.49(0.05)	0.58(0.07)	13.45	0.04(0.13)	0.51(0.32)	1.58(0.22)	<
16	J193555+194654	17.42(0.01)	1.03(0.02)	2.78(0.03)	14.64(0.03)	0.42(0.05)	0.56(0.07)	0.87(0.08)	13.77	0.03(0.17)	1.10(0.29)	1.33(0.28)	<
17	J194541+243253	15.20(0.10)	0.54(0.14)	1.53(0.11)	13.67(0.03)	0.23(0.05)	0.38(0.05)	0.69(0.07)	12.98	0.44(0.12)	1.11(0.14)	1.57(0.09)	8.36 0.15

Note. — Observed magnitudes and colors in the different IPHAS, 2MASS and IRAC bands, together with our measured 24- $\mu$ m fluxes from MIPS GAL images. The figures in brackets denote the 1  $\sigma$  uncertainties.

Table 7. Derived parameters for IPHAS A-type stars with 8- $\mu$ m excesses.

GLIPHAS No.	IPHAS ID	GLIMPSE ID	$A_r$ (mag)	d (kpc)	3.6 $\mu$ m (mJy)	4.5 $\mu$ m (mJy)	5.8 $\mu$ m (mJy)	8 $\mu$ m (mJy)	24 $\mu$ m (mJy)	T (K)	$L_{\text{IR}}/L_{\star}$
1	J190602+073418	G041.3305+00.2230	4.0 (0.2)	(0.8 0.2)	-	-	-	2.0 (7.0)	4.8 (9.0)	283 (24)	2.2e-03
2	J190650+090108	G042.7075+00.7117	6.0 (0.2)	(0.7 0.1)	-	-	-	13.7 (6.0)	-	$\leq 211$	-
3	J190952+070514	G041.3387-00.8442	5.5 (0.2)	(1.2 0.2)	-	-	-	5.3 (3.1)	-	$\leq 194$	-
4	J191100+094543	G043.8401+00.1431	4.4 (0.2)	(0.7 0.1)	14.3 (10.3)	20.1(11.8)	25.7 (18.5)	32.4 (33.5)	10.4(8.9)	654 (33)	8.5e-03
5	J191512+120907	G046.4350+00.3389	4.5 (0.3)	(2.0 0.4)	-	-	-	1.4 (7.1)	-	$\leq 243$	-
6	J191947+132707	G048.1073-00.0432	4.9 (0.2)	(1.9 0.4)	-	-	4.0 (5.3)	3.7 (7.1)	-	271 (63)	1.9e-02
7	J192227+141309	G049.0889-00.2538	3.5 (0.3)	(0.9 0.2)	-	-	-	5.1 (3.0)	$< 87.3$	$\leq 299$	-
8	J192612+163544	G051.6091+00.0765	3.5 (0.3)	(2.3 0.5)	-	-	-	0.6 (3.2)	-	$\leq 257$	-
9	J192914+184004	G053.7744+00.4315	3.1 (0.2)	(0.9 0.2)	-	-	2.1 (4.4)	8.6 (14.9)	19.9(9.2)	298 (20)	6.6e-03
10	J192933+183415	G053.7251+00.3191	2.5 (0.2)	(1.0 0.2)	3.3 (5.0)	3.1 (7.4)	3.4 (7.8)	7.0 (20.7)	15.6(9.6)	497 (57)	3.0e-03
11	J193110+164225	G052.2752-00.9138	5.1 (0.2)	(1.5 0.3)	-	-	-	1.3 (4.3)	$< 5.4$	$\leq 245$	-
12	J193117+185048	G054.1653+00.0894	4.2 (0.3)	(2.0 0.4)	-	-	1.3 (5.2)	1.1 (5.7)	$< 22.8$	455 (20)	4.3e-03
13	J193126+184131	G054.0455-00.0137	3.7 (0.2)	(1.2 0.3)	-	-	-	2.3 (4.4)	-	$\leq 183$	-
14	J193259+195709	G055.3273+00.2720	4.0 (0.3)	(1.7 0.4)	0.9 (3.2)	0.9 (3.0)	2.8 (6.8)	8.9 (11.3)	$< 46.9$	342 (43)	1.6e-02
15	J193516+195803	G055.6008-00.1905	2.9 (0.2)	(2.0 0.4)	-	-	-	1.0 (3.7)	-	$\leq 168$	-
16	J193555+194654	G055.5133-00.4151	3.8 (0.2)	(2.5 0.5)	-	-	-	0.7 (3.0)	$< 0.8$	$\leq 367$	-
17	J194541+243253	G060.7727-00.0227	1.9 (0.6)	(2.2 0.7)	-	0.8 (4.1)	1.6 (6.1)	1.5 (14.0)	3.3 (6.3)	482 (15)	3.8e-03

Note. — Derived parameters for stars with mid-IR excesses with respect to the SED of an A3V star normalised to the dereddened K-band fluxes. The excess fluxes listed for each wavelength are in mJy. The numbers in brackets denote the signal-to-noise ratios of the excess flux detections, except for the last column, where they represent  $1 \sigma$  uncertainties. Only detections with S/N ratios larger than 3.0 are shown. For each star, extinctions and distances were computed assuming all possible spectral types (A0-5), and the RMS value of each quantity was added quadratically to the photometric errors to derive the final uncertainties quoted here. For sources that show excess fluxes at more than one wavelength the infrared excess  $L_{\text{IR}}/L_{\star}$  are shown.



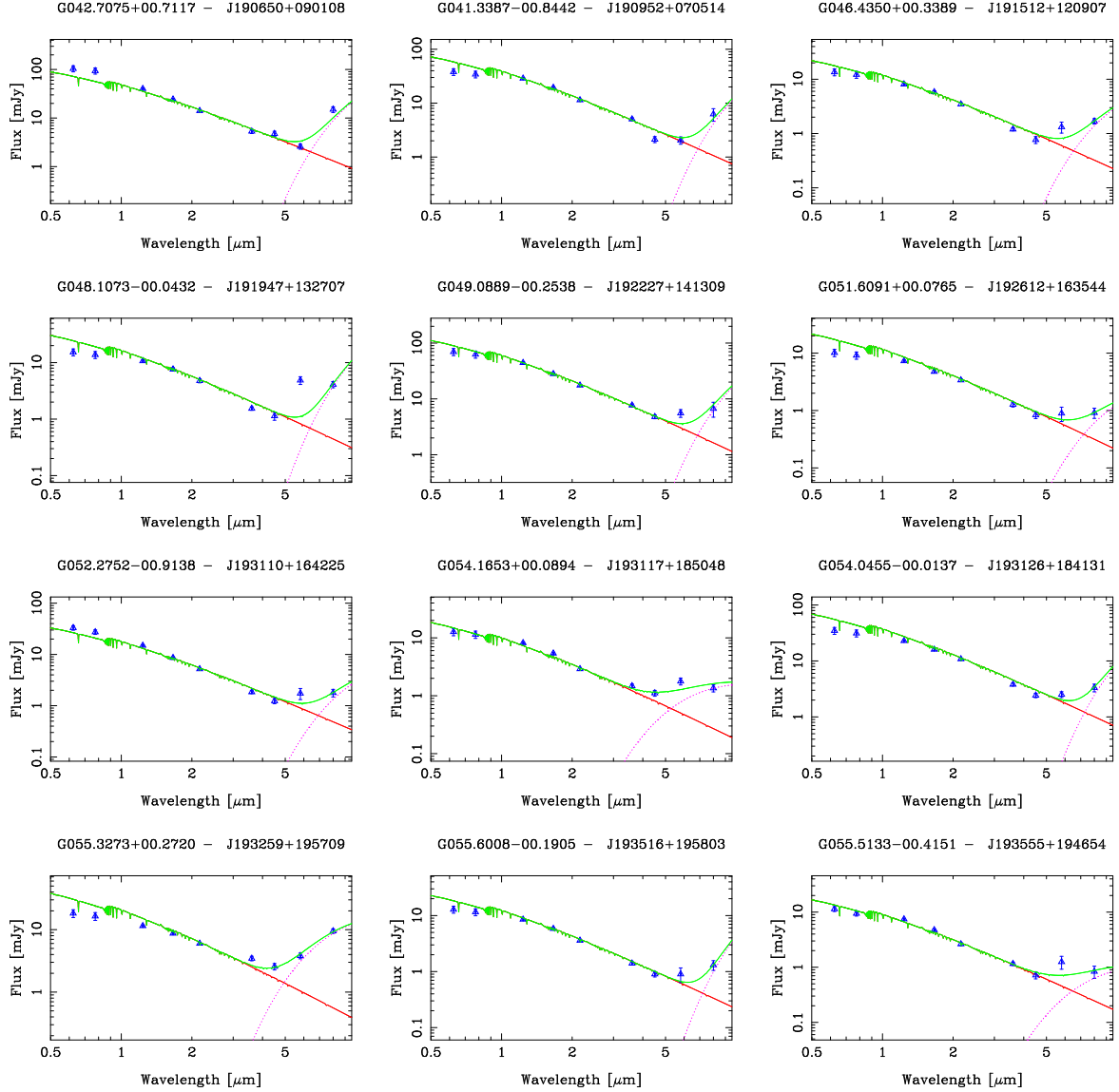


Fig. 7.— Dereddened optical IPHAS, 2MASS and GLIMPSE photometry for the IPHAS-selected A-type stars with 8- $\mu$ m excesses (blue triangles with error bars denoting the  $1\sigma$  photometric error of each measurement). For each star, the red solid line corresponds to the reference photospheric SED normalised to the K-band flux. The pink dotted line represents the black-body that, added to the stellar SED, minimizes the  $\chi^2$  fit to the data (solid green line). Only the 2MASS and GLIMPSE data points were included in the best-fitting routine.

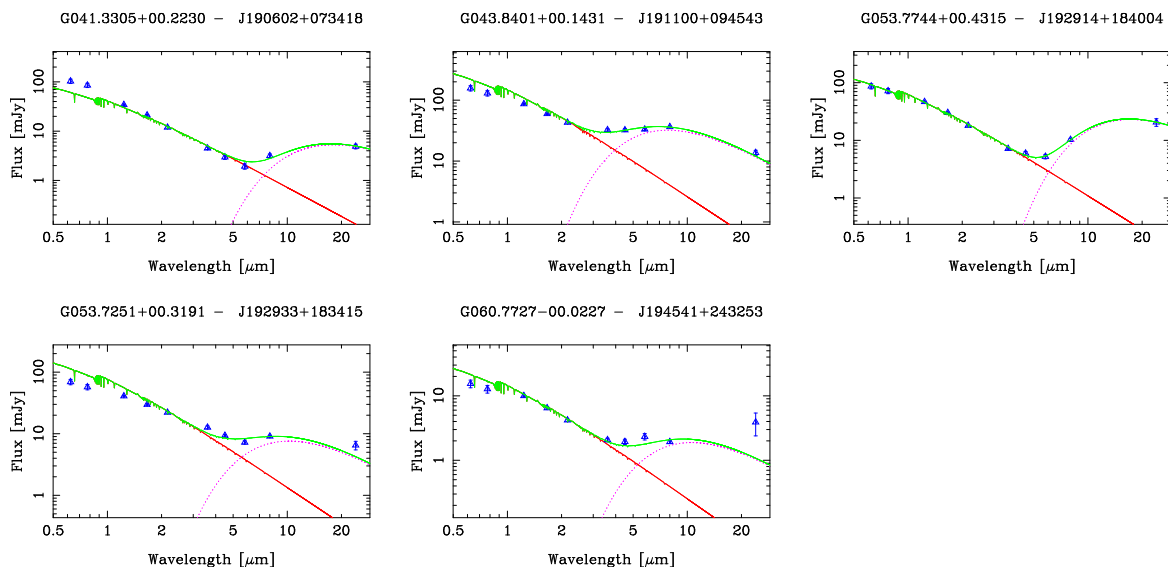


Fig. 8.— Dereddened optical IPHAS, 2MASS and GLIMPSE photometry for the IPHAS-selected A-type stars with excesses at  $8 \mu\text{m}$  and  $24 \mu\text{m}$  (blue triangles with error bars denoting the  $1\sigma$  photometric error of each measurement). For each star, the red solid line corresponds to the reference photospheric SED normalised to the K-band flux. The pink dotted line represents the black-body that, added to the stellar SED, minimizes the  $\chi^2$  fit to the data (solid green line). Only the 2MASS and GLIMPSE data points were included in the best-fitting routine.

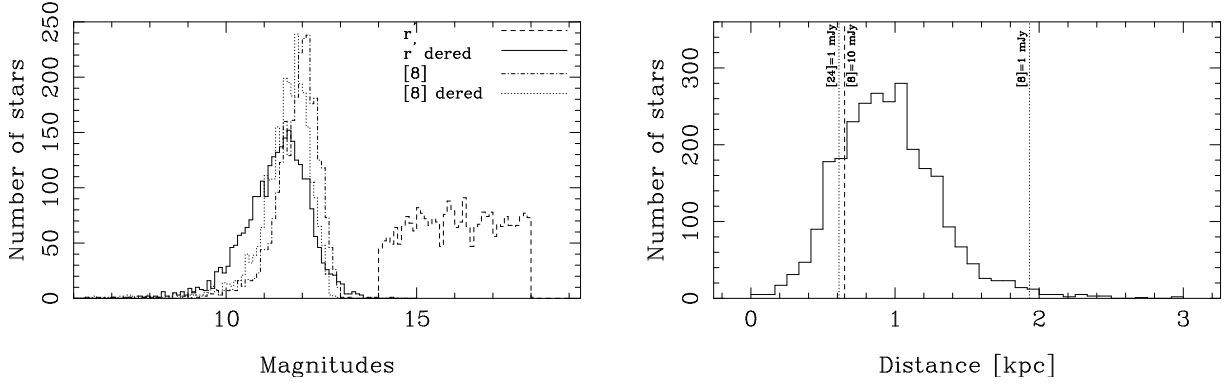


Fig. 9.— *Left-hand panel:* Distributions of observed and dereddened  $r'$  and  $[8]$  magnitudes for the 2692 A-type stars. After dereddening, good agreement between the IPHAS and Spitzer photometry is found, in accord with most stars being A-types. *Right-hand panel:* Histogram showing the distance distribution of the GLIPHAS sample, together with the IRAC  $8\text{-}\mu\text{m}$  and MIPS  $24\text{-}\mu\text{m}$  limiting distances for an unreddened A3V star. The dotted lines represent the limiting distances for detection of a 10 mJy and 1 mJy A3V star respectively, while the dashed line shows the 1 mJy MIPS limit. The limiting distances for unreddened A-type dwarfs in the IPHAS and 2MASS surveys fall well beyond the range of this plot ( $>20$  kpc and  $>4$  kpc, respectively).

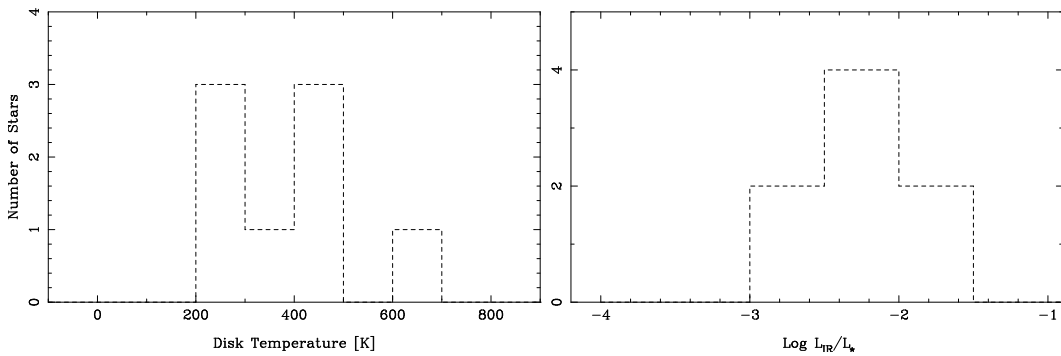


Fig. 10.— Distributions of best-fit blackbody dust temperatures (*left-hand panel*) and fractional infrared excesses ( $L_{\text{IR}}/L_*$ , *right-hand panel*) for sources with excesses at two or more wavelengths.

## REFERENCES

- Aumann, H. H. 1985, *PASP*, 97, 885
- Aumann, H. H., Beichman, C. A., Gillett, F. C., de Jong, T., Houck, J. R., Low, F. J., Neugebauer, G., Walker, R. G., & Wesselius, P. R. 1984, *ApJ*, 278, L23
- Aumann, H. H., & Probst, R. G. 1991, *ApJ*, 368, 264
- Backman, D. E., & Paresce, F. 1993, in *Protostars and Planets III*, ed. E. H. Levy & J. I. Lunine, 1253–1304
- Beichman, C. A., Bryden, G., Rieke, G. H., Stansberry, J. A., Trilling, D. E., Stapelfeldt, K. R., Werner, M. W., Engelbracht, C. W., Blaylock, M., Gordon, K. D., Chen, C. H., Su, K. Y. L., & Hines, D. C. 2005, *ApJ*, 622, 1160
- Benjamin, R. A., Churchwell, E., Babler, B. L., Bania, T. M., Clemens, D. P., Cohen, M., Dickey, J. M., Indebetouw, R., Jackson, J. M., Kobulnicky, H. A., Lazarian, A., Marston, A. P., Mathis, J. S., Meade, M. R., Seager, S., Stolovy, S. R., Watson, C., Whitney, B. A., Wolff, M. J., & Wolfire, M. G. 2003, *PASP*, 115, 953
- Benjamin, R. A., Churchwell, E., Babler, B. L., Indebetouw, R., Meade, M. R., Whitney, B. A., Watson, C., Wolfire, M. G., Wolff, M. J., Ignace, R., Bania, T. M., Bracker, S., Clemens, D. P., Chomiuk, L., Cohen, M., Dickey, J. M., Jackson, J. M., Kobulnicky, H. A., Mercer, E. P., Mathis, J. S., Stolovy, S. R., & Uzpen, B. 2005, *ApJ*, 630, L149
- Bohlin, R. C. 2007, in *Astronomical Society of the Pacific Conference Series*, Vol. 364, *The Future of Photometric, Spectrophotometric and Polarimetric Standardization*, ed. C. Sterken, 315
- Bronfman, L. 1992, in *Astrophysics and Space Science Library*, Vol. 180, *The Center, Bulge, and Disk of the Milky Way*, ed. L. Blitz, 131
- Bryden, G., Beichman, C. A., Trilling, D. E., Rieke, G. H., Holmes, E. K., Lawler, S. M., Stapelfeldt, K. R., Werner, M. W., Gautier, T. N., Blaylock, M., Gordon, K. D., Stansberry, J. A., & Su, K. Y. L. 2006, *ApJ*, 636, 1098
- Calvet, N., D’Alessio, P., Hartmann, L., Wilner, D., Walsh, A., & Sitko, M. 2002, *ApJ*, 568, 1008
- Cardelli, J. A., Clayton, G. C., & Mathis, J. S. 1989, *ApJ*, 345, 245

- Carey, S. J., Noriega-Crespo, A., Price, S. D., Padgett, D. L., Kraemer, K. E., Indebetouw, R., Mizuno, D. R., Ali, B., Berriman, G. B., Boulanger, F., Cutri, R. M., Ingalls, J. G., Kuchar, T. A., Latter, W. B., Marleau, F. R., Miville-Deschenes, M. A., Molinari, S., Rebull, L. M., & Testi, L. 2005, in *Bulletin of the American Astronomical Society*, 1252
- Carpenter, J. M. 2001, *AJ*, 121, 2851
- Cheng, K.-P., Bruhweiler, F. C., Kondo, Y., & Grady, C. A. 1992, *ApJ*, 396, L83
- Churchwell, E. B., Carey, S. J., & GLIMPSE Team. 2005, *American Astronomical Society Meeting Abstracts*, 206
- Cieza, L., et al. 2007, *ApJ*, 667, 308
- Clarke, A. J., Oudmaijer, R. D., & Lumsden, S. L. 2005, *MNRAS*, 363, 1111
- Cohen, M., Walker, R. G., Barlow, M. J., & Deacon, J. R. 1992, *AJ*, 104, 1650
- Currie, T., Kenyon, S. J., Balog, Z., Rieke, G., Bragg, A., & Bromley, B. 2008, *ApJ*, 672, 558
- Cutri, R. M., Skrutskie, M. F., van Dyk, S., Beichman, C. A., Carpenter, J. M., Chester, T., Cambresy, L., Evans, T., Fowler, J., Gizis, J., Howard, E., Huchra, J., Jarrett, T., Kopan, E. L., Kirkpatrick, J. D., Light, R. M., Marsh, K. A., McCallon, H., Schneider, S., Stiening, R., Sykes, M., Weinberg, M., Wheaton, W. A., Wheelock, S., & Zacarias, N. 2003, in *The IRSA 2MASS All-Sky Point Source Catalog*, NASA/IPAC Infrared Science Archive. <http://irsa.ipac.caltech.edu/applications/Gator/>
- D'Alessio, P., Calvet, N., & Hartmann, L. 2001, *ApJ*, 553, 321
- D'Alessio, P., Calvet, N., Hartmann, L., Lizano, S., & Cantó, J. 1999, *ApJ*, 527, 893
- D'Alessio, P., Canto, J., Calvet, N., & Lizano, S. 1998, *ApJ*, 500, 411
- D'Alessio, P., Hartmann, L., Calvet, N., Franco-Hernández, R., Forrest, W. J., Sargent, B., Furlan, E., Uchida, K., Green, J. D., Watson, D. M., Chen, C. H., Kemper, F., Sloan, G. C., & Najita, J. 2005, *ApJ*, 621, 461
- Drew, J. E., Greimel, R., Irwin, M. J., Aungwerojwit, A., Barlow, M. J., Corradi, R. L. M., Drake, J. J., Gänsicke, B. T., Groot, P., Hales, A., Hopewell, E. C., Irwin, J., Knigge, C., Leisy, P., Lennon, D. J., Mampaso, A., Mashedier, M. R. W., Matsuura, M., Morales-Rueda, L., Morris, R. A. H., Parker, Q. A., Phillipps, S., Rodriguez-Gil, P.,

- Roelofs, G., Skillen, I., Sokoloski, J. L., Steeghs, D., Unruh, Y. C., Viironen, K., Vink, J. S., Walton, N. A., Witham, A., Wright, N., Zijlstra, A. A., & Zurita, A. 2005, *MNRAS*, 362, 753
- Drew, J. E., Greimel, R., Irwin, M. J., & Sale, S. E. 2008, *MNRAS*, 386, 1761
- Dullemond, C. P., Hollenbach, D., Kamp, I., & D'Alessio, P. 2007, in *Protostars and Planets V*, ed. B. Reipurth, D. Jewitt, & K. Keil, 555
- Dunkin, S. K., Barlow, M. J., & Ryan, S. G. 1997, *MNRAS*, 290, 165
- Egan, M. P., Price, S. D., Shipman, R. F., & Tedesco, E. 1997, *BAAS*, 29, 1294
- Fajardo-Acosta, S. B., Beichman, C. A., & Cutri, R. M. 2000, *ApJ*, 538, L155
- Fazio, G. G., Hora, J. L., Allen, L. E., Ashby, M. L. N., Barmby, P., Deutsch, L. K., Huang, J.-S., Kleiner, S., Marengo, M., Megeath, S. T., Melnick, G. J., Pahre, M. A., Patten, B. M., Polizotti, J., Smith, H. A., Taylor, R. S., Wang, Z., Willner, S. P., Hoffmann, W. F., Pipher, J. L., Forrest, W. J., McMurty, C. W., McCreight, C. R., McKelvey, M. E., McMurray, R. E., Koch, D. G., Moseley, S. H., Arendt, R. G., Mentzell, J. E., Marx, C. T., Losch, P., Mayman, P., Eichhorn, W., Krebs, D., Jhabvala, M., Gezari, D. Y., Fixsen, D. J., Flores, J., Shakoordadeh, K., Jungo, R., Hakun, C., Workman, L., Karpati, G., Kichak, R., Whitley, R., Mann, S., Tollestrup, E. V., Eisenhardt, P., Stern, D., Gorjian, V., Bhattacharya, B., Carey, S., Nelson, B. O., Glaccum, W. J., Lacy, M., Lowrance, P. J., Laine, S., Reach, W. T., Stauffer, J. A., Surace, J. A., Wilson, G., Wright, E. L., Hoffman, A., Domingo, G., & Cohen, M. 2004, *ApJS*, 154, 10
- Gonzalez-Solares, E. A., Walton, N. A., Greimel, R., Drew, J. E., Irwin, M. J., Sale, S. E., Andrews, K., Aungwerojwit, A., Barlow, M. J., van den Besselaar, E., Corradi, R. L. M., Gaensicke, B. T., Groot, P. J., Hales, A. S., Hopewell, E. C., Hu, H., Irwin, J., Knigge, C., Lagadec, E., Leisy, P., Lewis, J. R., Mampaso, A., Matsuura, M., Moont, B., Morales-Rueda, L., Morris, R. A. H., Naylor, T., Parker, Q. A., Prema, P., Pyrzas, S., Rixon, G. T., Rodriguez-Gil, P., Roelofs, G., Sabin, L., Skillen, I., Suso, J., Tata, R., Viironen, K., Vink, J. S., Witham, A., Wright, N. J., Zijlstra, A. A., Zurita, A., Drake, J., Fabregat, J., Lennon, D. J., Lucas, P. W., Martin, E. L., Steeghs, D., & Unruh, Y. C. 2008, *MNRAS*, 388, 89
- Hayashi, C., Nakazawa, K., & Nakagawa, Y. 1985, in *Protostars and Planets II*, ed. D. C. Black & M. S. Matthews, 1100

- Hernández, J., Briceño, C., Calvet, N., Hartmann, L., Muzerolle, J., & Quintero, A. 2006, *ApJ*, 652, 472
- Horne, K. 1986, *PASP*, 98, 609
- Houk, N., Swift, C. M., Murray, C. A., Penston, M. J., & Binney, J. J. 1997, in *ESA SP-402: Hipparcos - Venice '97*, 279
- Hughes, A. M., Wilner, D. J., Kamp, I., & Hogerheijde, M. R. 2008, *ApJ*, 681, 626
- Indebetouw, R., Mathis, J. S., Babler, B. L., Meade, M. R., Watson, C., Whitney, B. A., Wolff, M. J., Wolfire, M. G., Cohen, M., Bania, T. M., Benjamin, R. A., Clemens, D. P., Dickey, J. M., Jackson, J. M., Kobulnicky, H. A., Marston, A. P., Mercer, E. P., Stauffer, J. R., Stolovy, S. R., & Churchwell, E. 2005, *ApJ*, 619, 931
- Irwin, M. J. 1985, *MNRAS*, 214, 575
- Kenyon, S. J., & Hartmann, L. 1995, *ApJs*, 101, 117
- Kurucz, R. L. 1979, *ApJS*, 40, 1
- Lagrange, A.-M., Backman, D. E., & Artymowicz, P. 2000, in *Protostars and Planets IV*, ed. V. Mannings, A. P. Boss, & S. S. Russell, 639
- Mannings, V., & Barlow, M. J. 1998, *ApJ*, 497, 330
- Meyer, M. R., Backman, D. E., Weinberger, A. J., & Wyatt, M. C. 2007, in *Protostars and Planets V*, ed. B. Reipurth, D. Jewitt, & K. Keil, 573
- Miller, G. E., & Scalo, J. M. 1979, *ApJS*, 41, 513
- Oke, J. B. 1990, *AJ*, 99, 1621
- Oudmaijer, R. D., van der Veen, W. E. C. J., Waters, L. B. F. M., Trams, N. R., Waelkens, C., & Engelsman, E. 1992, *A&AS*, 96, 625
- Pickles, A. J. 1998, *PASP*, 110, 863
- Plets, H., & Vynckier, C. 1999, *A&A*, 343, 496
- Rhee, J. H., Song, I., Zuckerman, B., & McElwain, M. 2007, *ApJ*, 660, 1556
- Rieke, G. H., Su, K. Y. L., Stansberry, J. A., Trilling, D., Bryden, G., Muzerolle, J., White, B., Gorlova, N., Young, E. T., Beichman, C. A., Stapelfeldt, K. R., & Hines, D. C. 2005, *ApJ*, 620, 1010

- Rieke, G. H., Young, E. T., Engelbracht, C. W., Kelly, D. M., Low, F. J., Haller, E. E., Beeman, J. W., Gordon, K. D., Stansberry, J. A., Misselt, K. A., Cadien, J., Morrison, J. E., Rivlis, G., Latter, W. B., Noriega-Crespo, A., Padgett, D. L., Stapelfeldt, K. R., Hines, D. C., Egami, E., Muzerolle, J., Alonso-Herrero, A., Blaylock, M., Dole, H., Hinz, J. L., Le Floch, E., Papovich, C., Pérez-González, P. G., Smith, P. S., Su, K. Y. L., Bennett, L., Frayer, D. T., Henderson, D., Lu, N., Masci, F., Pesenson, M., Rebull, L., Rho, J., Keene, J., Stolovy, S., Wachter, S., Wheaton, W., Werner, M. W., & Richards, P. L. 2004, *ApJS*, 154, 25
- Robitaille, T. P., Whitney, B. A., Indebetouw, R., & Wood, K. 2007, *ApJS*, 169, 328
- Russeil, D. 2003, *A&A*, 397, 133
- Sale, S. E., et al. 2008, arXiv:0810.2547
- Schlegel, D. J., Finkbeiner, D. P., & Davis, M. 1998, *ApJ*, 500, 525
- Schmidt-Kaler, T. 1982, in *Landolt-Bornstein: Numerical Data and functional Relationships in Science and Technology. New Series, Vol. 2b*, ed. K. Schaifers & H. H. Voigt (Springer, Berlin)
- Sicilia-Aguilar, A., Hartmann, L., Calvet, N., Megeath, S. T., Muzerolle, J., Allen, L., D’Alessio, P., Merín, B., Stauffer, J., Young, E., & Lada, C. 2006, *ApJ*, 638, 897
- Silverstone, M. D. 2000, Ph.D. Thesis, University of California
- Silverstone, M. D., Meyer, M. R., Mamajek, E. E., Hines, D. C., Hillenbrand, L. A., Najita, J., Pascucci, I., Bouwman, J., Kim, J. S., Carpenter, J. M., Stauffer, J. R., Backman, D. E., Moro-Martin, A., Henning, T., Wolf, S., Brooke, T. Y., & Padgett, D. L. 2006, *ApJ*, 639, 1138
- Smith, P. S., Hines, D. C., Low, F. J., Gehrz, R. D., Polomski, E. F., & Woodward, C. E. 2006, *ApJ*, 644, L125
- Song, I., Caillault, J.-P., Barrado y Navascués, D., & Stauffer, J. R. 2001, *ApJ*, 546, 352
- Su, K. Y. L., Rieke, G. H., Stansberry, J. A., Bryden, G., Stapelfeldt, K. R., Trilling, D. E., Muzerolle, J., Beichman, C. A., Moro-Martin, A., Hines, D. C., & Werner, M. W. 2006, *ApJ*, 653, 675
- Sylvester, R. J., & Mannings, V. 2000, *MNRAS*, 313, 73
- Sylvester, R. J., Skinner, C. J., Barlow, M. J., & Mannings, V. 1996, *MNRAS*, 279, 915



- Uzpen, B., Kobulnicky, H. A., Olsen, K. A. G., Clemens, D. P., Laurant, T. L., Meade, M. R., Babler, B. L., Indebetouw, R., Whitney, B. A., Watson, C., Wolfire, M. G., Wolff, M. J., Benjamin, R. A., Bania, T. M., Cohen, M., Devine, K. E., Dickey, J. M., Heitsch, F., Jackson, J. M., Marston, A. P., Mathis, J. S., Mercer, E. P., Stauffer, J. R., Stolovy, S. R., Backman, D. E., & Churchwell, E. 2005, *ApJ*, 629, 512
- Uzpen, B., Kobulnicky, H. A., Monson, A. J., Pierce, M. J., Clemens, D. P., Backman, D. E., Meade, M. R., Babler, B. L., Indebetouw, R., Whitney, B. A., Watson, C., Wolfire, M. G., Benjamin, R. A., Bracker, S., Bania, T. M., Cohen, M., Cyganowski, C. J., Devine, K. E., Heitsch, F., Jackson, J. M., Mathis, J. S., Mercer, E. P., Povich, M. S., Rho, J., Robitaille, T. P., Sewilo, M., Stolovy, S. R., Watson, D. F., Wolff, M. J., & Churchwell, E. 2007, *ApJ*, 658, 1264
- Uzpen, B., Kobulnicky, H. A., & Kinemuchi, K. 2008, arXiv:0812.2847
- Valdes, F., Gupta, R., Rose, J. A., Singh, H. P., & Bell, D. J. 2004, *ApJS*, 152, 251
- Walker, H. J., & Wolstencroft, R. D. 1988, *PASP*, 100, 1509
- Waters, L. B. F. M., & Waelkens, C. 1998, *ARA&A*, 36, 233
- Witham, A. R., Knigge, C., Drew, J. E., Greimel, R., Steeghs, D., Gaensicke, B. T., Groot, P. J., & Mampaso, A., 2008, *MNRAS*, 384, 1277
- Wright, C. O., Egan, M. P., Kraemer, K. E., & Price, S. D. 2003, *AJ*, 125, 359
- Wuchterl, G., Guillot, T., & Lissauer, J. J. 2000, in *Protostars and Planets IV*, ed. V. Mannings, A. P. Boss, & S. S. Russell, 1081
- Zuckerman, B. 2001, *ARA&A*, 39, 549